

Vol. 21 • No. 5 • March 8 • 2011

www.afm-journal.de

ADVANCED FUNCTIONAL MATERIALS

Carbide-Derived Carbons – From Porous Networks to Nanotubes and Graphene

Volker Presser, Min Heon, and Yury Gogotsi*

Carbide-derived carbons (CDCs) are a large family of carbon materials derived from carbide precursors that are transformed into pure carbon via physical (e.g., thermal decomposition) or chemical (e.g., halogenation) processes. Structurally, CDC ranges from amorphous carbon to graphite, carbon nanotubes or graphene. For halogenated carbides, a high level of control over the resulting amorphous porous carbon structure is possible by changing the synthesis conditions and carbide precursor. The large number of resulting carbon structures and their tunability enables a wide range of applications, from tribological coatings for ceramics, or selective sorbents, to gas and electrical energy storage. In particular, the application of CDC in supercapacitors has recently attracted much attention. This review paper summarizes key aspects of CDC synthesis, properties, and applications. It is shown that the CDC structure and properties are sensitive to changes of the synthesis parameters. Understanding of processing–structure–properties relationships facilitates tuning of the carbon material to the requirements of a certain application.

1. Introduction

In parallel with the rise of nanomaterial research and applications, interest in carbons as multipurpose materials has spiked in recent years.^[1,2] One field in particular has attracted attention: carbon materials for energy-related applications such as batteries, supercapacitors, fuel cells, and gas storage.^[1] It is necessary to understand the relationship between carbon structure and the resulting properties to be able to tune and optimize the carbon material to meet application requirements. With carbon materials existing in a variety of forms (amorphous and crystalline; sp^2 and sp^3 hybridization; porous and dense; films, particles, nanotubes, and fibers) numerous applications are possible,^[2] but selecting the best material for a specific application may be challenging.

Porous carbons, fullerenes, nanotubes and, more recently, graphene are among the most widely studied materials. While there are numerous methods of synthesizing carbon materials from gaseous, solid, and liquid precursors, their synthesis

from carbides has attracted special attention lately.^[3,4] Carbide-derived carbons (CDCs) encompass a large group of carbons ranging from extremely disordered to highly ordered structures (Figure 1). The carbon structure that results from removal of the metal or metalloid atom(s) from the carbide depends on the synthesis method (halogenation, hydrothermal treatment, vacuum decomposition, etc.), applied temperature, pressure, and choice of carbide precursor.

The growing interest in this field is reflected by a rapidly increasing number of publications and patents. A significant progress in CDC research has been seen in several fields. Various carbide precursors have been systematically studied. Studies on binary carbides with different grain sizes show the possibility of low-temperature carbon formation for nanopowders.

Also, a better understanding of graphene formation during high-temperature vacuum decomposition of silicon carbide has been achieved since SiC single crystals are now available in large sizes with extremely low defect concentrations and an almost atomically flat surface finish.^[8]

CDC applications as electrode materials in electric double layer capacitors have attracted much attention lately.^[9] The unique properties of porous CDC obtained by halogenation, such as a high specific surface area and tunable pore size with a narrow size distribution, make it an ideal material for sorbents or supercapacitor electrodes. CDCs have been derived from many precursors (SiC, TiC, Mo_2C , VC, etc.) using a variety of treatment conditions that lead to a broad range of useful properties. Furthermore, graphene,^[10] nanotubes,^[11] and even nanodiamond^[12] can be produced from carbide precursors. Their applications naturally differ from those of porous CDC.

The last comprehensive journal review on this subject was published about fifteen years ago in Russian;^[13] book chapters published later^[3,4,14] are less accessible and require updating due to rapid progress in the field over the past few years. The most recent review of CDC^[14] covers only energy-related applications. Therefore, a comprehensive review on the field is long overdue. The goal of this article is to show how a variety of carbon structures can be produced from carbides, to explain how those structures can be controlled on the nanometer and subnanometer scale, and to describe CDC properties that are beneficial for a number of applications.

V. Presser, M. Heon, Prof. Y. Gogotsi
Department of Materials Science & Engineering and A.J. Drexel
Nanotechnology Institute
Drexel University
3141 Chestnut St., Philadelphia, PA 19104, USA
E-mail: gogotsi@drexel.edu

DOI: 10.1002/adfm.201002094

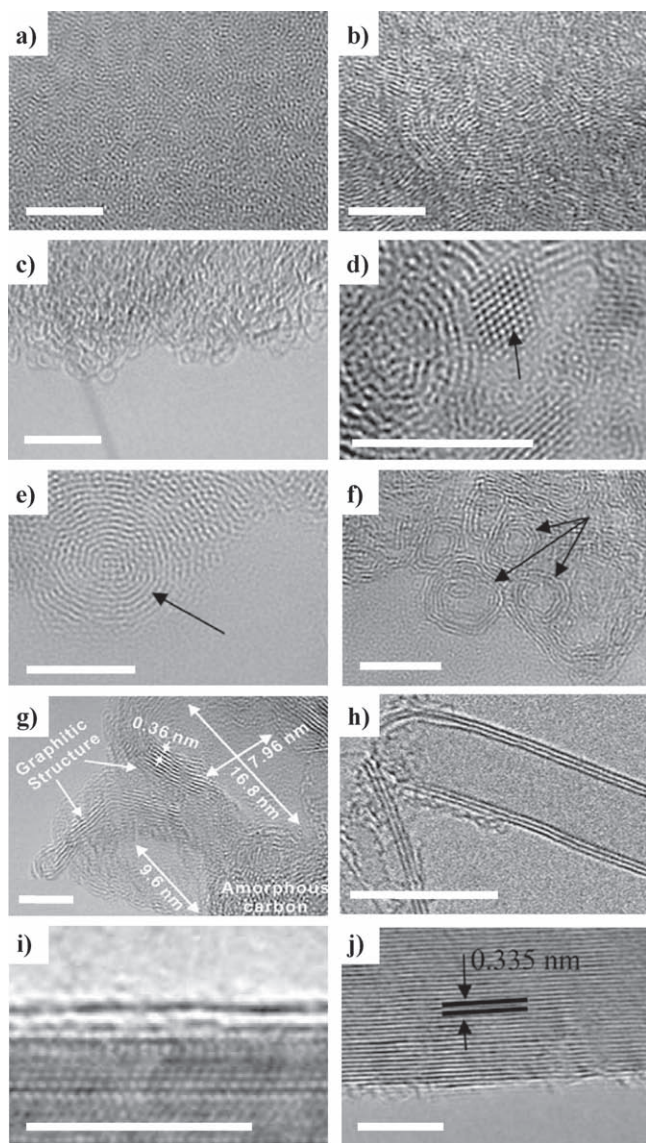


Figure 1. Transmission electron microscopy images of various CDC structures as obtained from carbide chlorination^[4,5] (a–g, j) and vacuum decomposition of SiC^[6,7] (h–i). Amorphous porous carbon (a), turbostratic carbon (b), fullerene-like carbon (c), nano-diamond (d), onion-like carbon (e), carbon nano-barrels (f), mesoporous carbon (g), carbon nanotubes (h), epitaxial graphene (i), graphite (j). The scale bar is 5 nm. Reproduced with permission.^[4] Copyright 2006, CRC Taylor & Francis. Reproduced with permission.^[5–7] Copyright 2008–2010, Elsevier.

2. Nomenclature

Over the years, different terms were used for CDCs, such as “mineral carbons”^[15] or “nanoporous carbons” (NPC).^[13] While the former has been out of use for a long time, the latter does not reflect the variety of carbon structures present in the CDC family and does not differentiate between CDC and an activated or template carbon with nanoscale porosity. In recent years, most studies refer to CDC using a nomenclature that clearly indicates the carbide precursor. Silicon carbide-derived



Volker Presser received his PhD from the Eberhard Karls Universität in Tübingen, Germany. Being awarded the Feodor Lynen Research Fellowship from the Alexander von Humboldt Foundation, he joined Drexel University, Philadelphia, as a post-doctoral researcher in 2010. As the leader of the carbide-derived carbons group, he investigates the correlation

between structure and properties of carbon nanomaterials.



Min Heon is a PhD student at Drexel University. He received his B.S. and M.S. degrees in Materials Science and Engineering from Pohang University of Science and Technology (POSTECH) in Korea and worked for Samsung Corning as a research engineer for eight years developing materials and devices related to LCD

display technologies. His research is concerned with new devices for electric energy storage and he explores patterned carbide-derived carbon films for application in micro-supercapacitors.



Yury Gogotsi is Distinguished University Professor and Trustee Chair in the Department of Materials Science and Engineering at Drexel University. He also serves as director of the A.J. Drexel Nanotechnology Institute. He received his MS (1984) and PhD (1986) degrees from Kiev Polytechnic and a DSc degree from

the Ukrainian Academy of Science in 1995. His current research is focused on carbon nanomaterials.

carbon, for example, has been referred to as SiC-CDC,^[16] SiC-DC,^[17] Si-CDC,^[18] or SiCDC. Since the latter two, however, do not indicate the different stoichiometries of the precursor (e.g., B₄C, TiC_{0.5}, or WC vs. W₂C) and are not applicable to carbons derived from carbonitrides (e.g., SiCN) and other complex compounds, they should not be used. We will use the “precursor-CDC” terminology and recommend its use in future

publications as the most descriptive term. This nomenclature can also be used for a more general description of precursor type, such as PDC-CDC (polymer-derived ceramics). For CDC derived from ordered mesoporous (OM) carbide precursors, the nomenclature OM-CDC was introduced^[19] in analogy to OM-SiC.^[20] In this regard, we suggest using a more specific term, like OM-SiC-CDC, which clearly indicates the precursor and not just the resulting structure.

3. CDC Synthesis and Structure

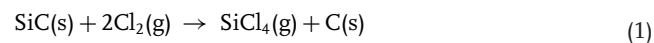
Several chemical reactions and physical processes can be used for CDC synthesis. Halogenation and especially chlorination has become one of the key synthetic methods for large-scale production of CDC. All CDC synthesis methods have one aspect in common: carbon is formed by selective extraction of the metal or metalloid atoms, transforming the carbide structure into pure carbon. In this way, the carbon layer is formed by inward growth, usually with the retention of the original shape and volume of the precursor. If the remaining reaction products (e.g., metal chlorides) are trapped in the pores, they can be removed by subsequent treatment such as hydrogenation or vacuum annealing. While CDC grows into the substrate carbide, other carbon-forming processes used for manufacturing carbon films (chemical or physical vapor deposition: CVD, PVD) coat the film onto an existing substrate (bottom-up versus top-down approach, respectively).

CDC can be formed from carbide precursors by many different methods, including acid etching or reactions with inorganic salts; however, chemical extraction of the metal atom(s) via halogenation, hydrothermal treatment, and vacuum decomposition are the most common chemical reactions leading to carbon formation and they will be discussed in detail in the following sections.

3.1. Halogenation

3.1.1. Historic Perspective and Carbide Precursors

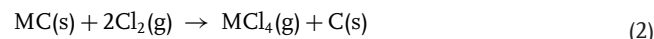
Selective extraction of metal atoms from the carbide lattice was reported at elevated temperatures (typically above 200 °C) and ambient pressure for many carbides. Chlorination of silicon carbide, originally patented by Otis Hutchins in 1918, was the first reported method of producing CDC.^[21] By exposing hot silicon carbide to dry chlorine gas, the formation of silicon tetrachloride and residual carbon was observed following Equation 1:



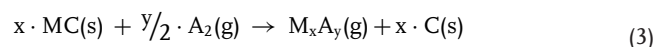
Slightly modified in 1956,^[22] this process was widely used for large-scale synthesis of SiCl₄ before pure silicon became abundantly available as a result of the advent of the modern semiconductor industry. Initially regarded as merely an undesired byproduct of SiCl₄ synthesis produced in ton quantities, it was later realized that porous CDC was a new class of carbon.^[15] The novelty and the name “mineral carbon”^[15] were justified in terms of structure (chlorination usually produced highly disordered porous carbon) and absence of organic residues,

unlike that in activated carbon. Remaining residual chlorine or metal chlorides can be removed by annealing, for example, in hydrogen gas. From the experience of large-scale SiCl₄ synthesis, it is clear that CDC synthesis process can be easily scaled up to manufacturing commercial quantities of carbon per year.

For many binary carbides (e.g., M = Si, Ti, Zr), Equation 2 yields both gaseous MCl₄ and solid carbon in the temperature range of interest:^[23–25]



The carbon formation by selective carbide etching is possible for other binary carbides and different halogens^[26–30] leading to a more general reaction equation:



where A is a gaseous halogen (F₂, Cl₂, Br₂, I₂, or mixtures thereof) or a halogen-containing etchant (e.g., HCl, HF), and M_xA_y a gaseous reaction product.

Fluorination with F₂, or with a milder agent (e.g., CoF₃), was shown to etch a large number of carbides (Al₄C₃, B₄C, CaC₂, Cr₃C₂, Fe₃C, SiC, ThC₂, TiC, UC₂, WC) and fluorocarbons were identified as a solid reaction product.^[31] Direct fluorination was found to be very aggressive, either producing fluorocarbons from carbides^[31] or leading to the disintegration of SiC thin films.^[32] Non-fluorinated SiC-CDC was described in the case of XeF₂ etching, offering a method of low-temperature synthesis (120 °C)^[32] as an alternative to SiC chlorination, which is usually carried out at much higher temperatures.^[4]

For ternary carbides, more complex reaction equations must be written. For example, when considering Ti₃SiC₂ we must be aware that partial chlorination may yield more solid reaction products, namely silicon carbide and titanium carbide, along with carbon.^[33] The same was discussed for Ti₂AlC.^[34] Some metal chlorides, for example, CaCl₂, have a high melting point (*T*_m = 782 °C) and may be present as solid reaction products.

A large number of binary and ternary carbides have been used for CDC synthesis: Al₄C₃, B₄C, BaC₂, CaC₂, Cr₃C₂, Fe₃C, Mo₂C, MoC, Nb₂C, NbC, SiC, SrC₂, Ta₂C, TaC, Ti₂AlC, Ti₃AlC₂, Ti₃SiC₂, TiC, VC, W₂C, WC, and ZrC.^[18,23,33–58] Using the same technique and temperatures as for carbide chlorination, porous CDC nanostructures were also reported for, e.g., carbonitrides, carbide-nitride composites, such as ZrC/ZrN^[15] and SiC/Si₃N₄^[5] or carbon and metal containing substances other than carbides such as ferrocene (Fe(C₅H₅)₂).^[59–61]

Many kinds and shapes of CDC materials have been formed via halogenation of such precursors: ceramic bodies obtained by sintering,^[62] or hot-pressing,^[24] whiskers,^[30] thin films,^[41,63] and both micro- and nanometer-sized powders,^[29,42,45] as well as single crystals.^[61] With large, high quality silicon carbide single crystals^[64] and high-quality carbide thin films^[65] widely available, a number of fundamental studies have been carried out and have greatly enhanced our understanding of CDC formation. The use of high-purity materials in the form of single crystals or thin films eliminates complications caused by the presence of sintering aids and high defect or impurity concentrations in ceramic materials.

Chlorination is the most economic and scalable method for CDC synthesis. Two companies, Y-Carbon (located near Philadelphia, USA) and Skeleton Technologies (located in Tartu, Estonia) produce CDC as their main product and are in the process of scaling up the production. A number of other companies, however, produce CDC as a byproduct of metal chloride synthesis. Production costs can be further reduced when chlorination is performed in a closed-loop system in which the reaction product (e.g., TiCl_4) is recycled and turned back into metal carbide, such as TiC . The costs can also be lowered by utilizing high-purity chlorides (SiCl_4 , TiCl_4 , or MoCl_5) produced along with CDC. There is a high demand for these chlorides, especially TiCl_4 , because hydrolysis of titanium tetrachloride is the most common commercial route to the synthesis of TiO_2 , as either nanometer or micrometer-sized particles,^[66] for photocatalytic and other applications.

3.1.2. Thermodynamics of Carbide Reactions with Halogens

Thermodynamic analysis of chlorination of SiC ,^[3,67] Ti_3AlC_2 ,^[34] Ti_2AlC ,^[33] TiC ,^[3] and ZrC ^[51] has been reported and has helped to understand what kind of reactions can lead to carbon formation, and the effect of temperature, pressure and concentration on the formation of carbon. The two most important factors of thermodynamic significance are the treatment temperature and the chlorine-to-carbide ratio, χ . From calculations, it is evident that the halogen species must be present at an excess amount to produce carbon without residual solids (TiC , SiC , etc.) even at temperatures as high as 1200 °C (Figure 2).

It was also suggested that carbon formation from binary^[51] and ternary carbides^[34] is possible even at room temperatures where carbon is not the only solid phase in the reaction (Figure 2a) and a high content of unreacted carbide is present.

For CDC formation, we can identify three different temperature ranges.^[51] In the low temperature range I, no CDC formation is predicted because of the preferred formation of CCl_4 . At moderate temperatures, both CCl_4 and carbon formation can be observed (range II). In the high temperature range III, solid carbon is the only stable carbon-containing reaction product. With an increased chlorine to carbon ratio, the onset of carbon formation and maximum carbon yield (range III) shifts to higher temperatures. From those calculations, it is clear that there is an optimum value for χ , corresponding to a large range over which a maximum yield of pure carbon as the only stable reaction product can be observed. High values for χ shift the onset of range III to high temperatures and low values of χ result in unreacted carbide or in decreased yield because of the presence of CCl_4 .

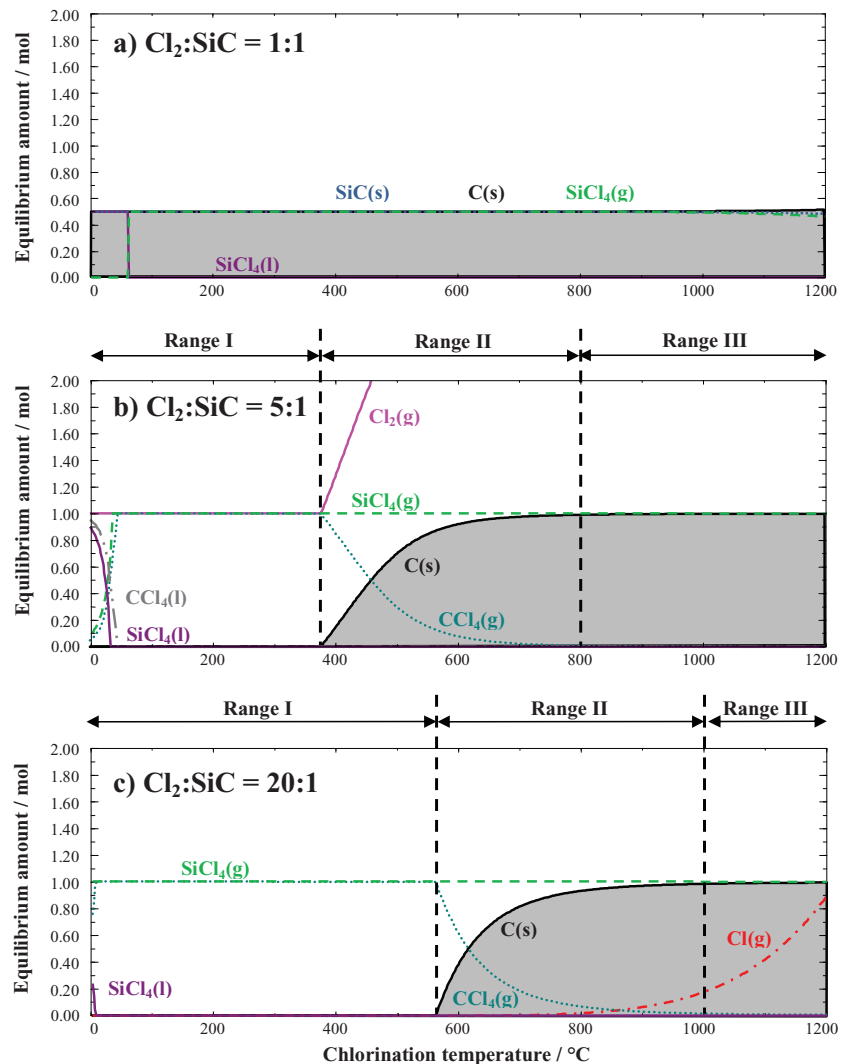


Figure 2. Thermodynamic calculations for the chlorination of silicon carbide with different carbide to chlorine ratios. Chlorine to carbide ratio of 1:1 (a), 5:1 (b), and 20:1 (c).

While thermodynamic calculations provide valuable information on CDC formation under equilibrium conditions in a closed system, the typical apparatus for carbide chlorination is an open system in which gaseous reaction products are continuously removed in a steady flow of chlorine-containing gas, shifting Equation 3 to the right and favoring carbon formation. Thus, thermodynamic calculations should be considered as a guideline suggesting that maximum yield of carbon can be observed at moderate temperatures for moderate chlorine-to-carbide ratios.

3.1.3. Reaction Kinetics

CDC growth can usually be described with a linear growth rate (k_l)^[25,68] for porous films up to approximately 50–100 μm thickness,^[26,27,69,70] indicating a reaction-controlled mechanism (Figure 3a). This is in contrast to oxidation of, for example, silicon carbide,^[71] which obeys a parabolic growth law for layers thicker than 2 nm after an initial linear growth phase. The linear growth

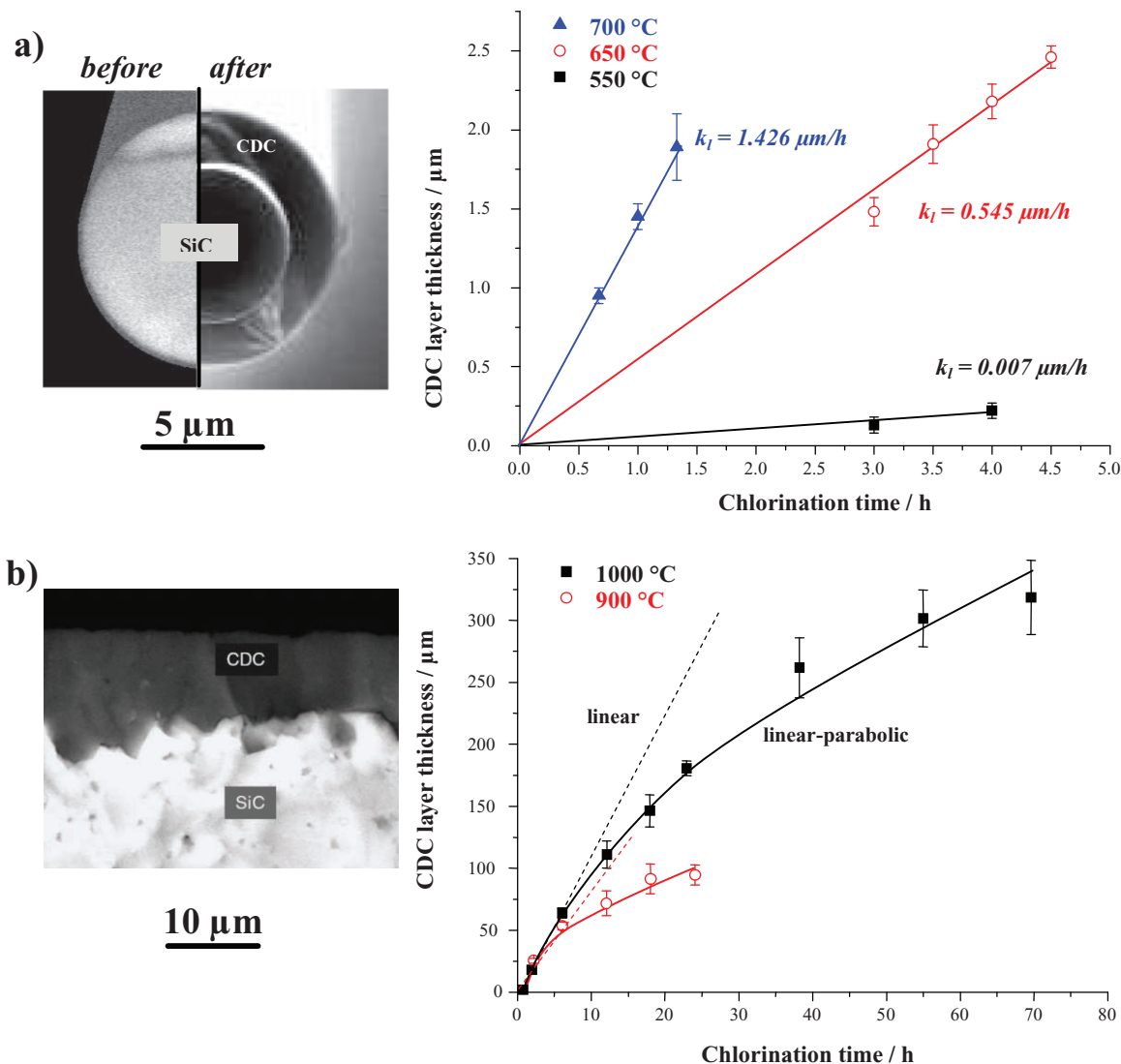


Figure 3. Growth kinetics of CDC films during chlorination of Tyranno SiC fibers^[69] in pure Cl₂ (a) and sintered α -SiC^[45] in Ar + 3.5% Cl₂ (b). As seen, for a short time and at low temperatures, linear kinetics are observed. For thicker CDC films, the parabolic time law is clearly visible. Panel (a) reproduced with permission.^[69] Copyright 2003, John Wiley and Sons. Panel (b) reproduced with permission.^[45] Copyright 2006, Institute of Physics.

of CDC films results from the high porosity of the CDC layer (see section 2.1.4). Micropores (<2 nm) provide an accessible network for the outward diffusion of the SiCl₄ molecule (0.568 nm). In this way, carbide fibers,^[69,72] films,^[73] plates,^[74] and powders^[51] can be completely transformed into CDC by halogenation.

For thicker CDC layers and longer halogenation times, linear-parabolic Deal-and-Grove-like growth kinetics indicating a diffusion-controlled mechanism have been reported.^[49,69] It is possible to fit the CDC film growth data reasonably well with a linear regression (Figure 3b) up to approximately 80 μm for chlorination at 1000 °C and up to 50 μm at 900 °C (Ar + 1.04 wt% Cl₂).^[45] With the diffusion kinetics following an Arrhenius temperature dependency, the linear regime of CDC formation becomes narrower at lower temperatures.

In steady-flow chlorination, the gas flow rate was shown to have a significant influence on the halogenation rate. Orekhov et al.^[25]

determined the chlorination rate of ZrC and found constant k_l -values ($\pm 5\%$) above ~ 6 mm/s gas flow and an abrupt decrease by a factor of 2 in the CDC rate at values below that. The rate change can be explained by the thermodynamic calculations presented in Figure 2: a decrease in the chlorine gas pressure creates a local atmosphere near the carbide surface causing the chlorination rate to drop. The chlorination rate also depends on the geometry of the chlorination apparatus and the sample type. For example, densely packed thick layers of carbide powder may require higher flow rates and/or longer chlorination times than thin films. This is in agreement with a recent study on TiC-CDC formation kinetics where the conversion rate was found to be a function of chlorine concentration following a Langmuir-Hinshelwood equation.^[68] The most important aspect of CDC formation, however, is that with a well-calibrated temperature and time dependency, it is possible to control the CDC film thickness with high accuracy.

Changing the halogen concentration in the gas phase will also result in a different CDC formation rate. For example, adding hydrogen to pure chlorine gas was shown to slow down the net reaction rate of SiC chlorination considerably (a decrease of 22% for every 1% H₂ addition to Cl₂ at 1000 °C^[75]). Additionally, a direct relation between the fluorine partial gas pressure and the resulting fluorination rate of ZrC was reported by Kuriakose et al.^[27]

When performing carbide halogenation at different temperatures, the activation energy E_a of CDC formation can be calculated using an Arrhenius equation. For the chlorination of TiC (NbC), an activation energy of 50 (38) kJ mol⁻¹ was reported by Kirillova et al.^[23] in the temperature range between 400–800 °C. Kuriakose et al. calculated an activation energy of 92 kJ mol⁻¹ for fluorination of ZrC and HfC in the range of 300–900 °C. For ZrC chlorination at higher temperatures, there is a large decrease in the activation energy from 62 kJ/mol (450–650 °C) to a very low value of 10 kJ/mol (650–950 °C). A similar but less drastic decrease in E_a is seen in the data presented by Zelikman et al.^[49] for WC: 153 kJ mol⁻¹ between 600 °C and 750 °C, and 42 kJ mol⁻¹ between 750 °C and 980 °C. For TiC under the same conditions, no such change in the activation energy was reported and a constant E_a of 23 kJ mol⁻¹ (650–900 °C) was found. This could be explained in terms of reaction control: at higher temperatures, the lower activation energy is caused by the predominance of the reaction itself (corresponding to linear kinetics), while at lower temperatures CDC formation is diffusion-controlled (corresponding to parabolic kinetics). Values above 100 kJ mol⁻¹ are in the range of typical diffusion-related activation energies (e.g., 113 kJ mol⁻¹ for O₂ diffusion in silica glass^[76]). This is corroborated by the reported value of $E_a = 144$ kJ mol⁻¹ for the parabolic CDC layer growth on SiC at 900–1000 °C.^[69]

3.1.4. Conformal Carbide-to-Carbon Transformation

CDC formation by carbide halogenation typically maintains the original shape and volume of the carbide precursor and is, therefore, referred to as a conformal transformation process.^[69,70] This phenomenon was first reported for TiC powder where grain size and shape did not change as a result of chlorination.^[43] A recent transmission electron microscopy (TEM) study on CDC synthesis showed that the net shape of even a complex shaped carbide precursor is maintained after chlorination of β -SiC whiskers.^[30] This conformal transformation is shown in Figure 4 where a β -SiC precursor is gradually consumed by the forming CDC layer until the entire whisker has been fully transformed.

Due to their extremely high porosity (>75 vol%), a partial collapse of the carbon structure and resulting cracks were reported for micrometer sized powders of CDC from ternary carbides (Ti₃AlC₂, Ti₂AlC) and carbonitrides, (Ti₂AlC_{0.5}N_{0.5}).^[33] Although largely conformal, some shrinkage was observed along the *a*-axis (Figure 5a) in which the density of carbon atoms is lower. This phenomenon is a limitation for CDC synthesis from thin films or for manufacturing thick free-standing CDC plates from certain carbides. For refractory bodies or thin films, crack formation or structural collapse may occur for CDC with a porosity larger than 68–74 vol%, as predicted by the structural stability criterion of highly porous ceramics calculated by Pabst et al.^[77]

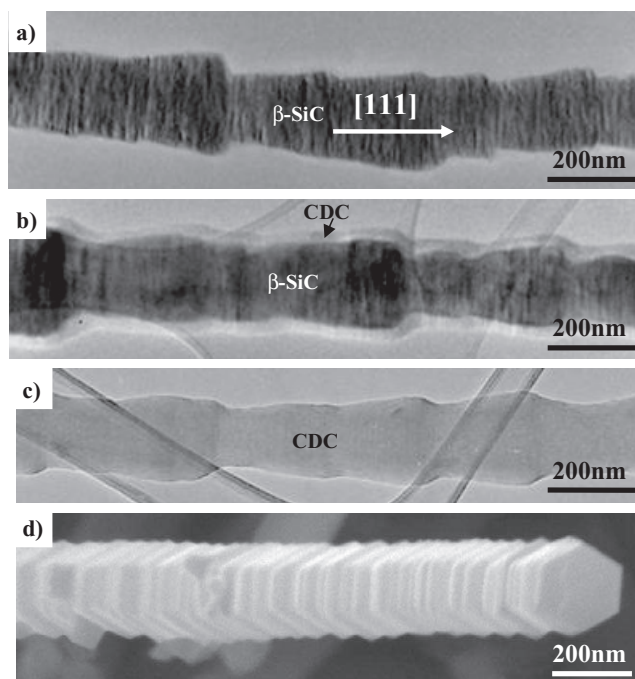


Figure 4. TEM (a–c) and SEM (d) images showing a comparison of 3C-SiC (β -SiC) whiskers at various stages of chlorination: as received (a), chlorinated at 700 °C (b) and 1200 °C (c). Shape and size of the initial whisker are largely maintained after silicon carbide halogenation (d). The diagonal structures seen in Figure 4b and c originate from the TEM grid (lacey carbon). Reproduced with permission.^[30] Copyright 2006, The American Ceramic Society.

The conformal carbide-carbon transformation can also be observed when using polymer-derived carbides (PDC), such as polycarbosilane-derived silicon carbide^[72] or polymer-derived silicon carbonitride,^[5] as precursors. While net shape and size changes can be observed when comparing the precursor and the material after pyrolysis, only minimal changes result from subsequent halogenation. Biomorphic porous carbon is a special form of template that can be obtained from carbonized paper and readily reacts with methane and TiCl₄ to form mesoporous TiC.^[78] This mesoporous TiC also undergoes conformal transformation to CDC upon chlorination.^[78,79] Conformal transformation into carbon allows CDC formation to be carried out partially, producing metal carbides coated with carbon that have catalytic, tribological and other applications.

3.1.5. Porosity, Pore Size Distribution (PSD) and Specific Surface Area (SSA)

A high bulk porosity (>50 vol%) with a high specific surface area (SSA more than 2000 m² g⁻¹) is characteristic of CDC obtained via halogenation.^[3-5,9,37] The bulk porosity of CDC is largely determined by the carbide structure. When metal atoms are extracted from the carbide lattice, the remaining carbon forms microporous CDC structures. This is schematically illustrated in Figure 5 for Ti₃SiC₂ and 3C-SiC. Figure 5 shows that differences in the distribution of carbon atoms in the carbide lattice lead to a major change in the resulting CDC structure.

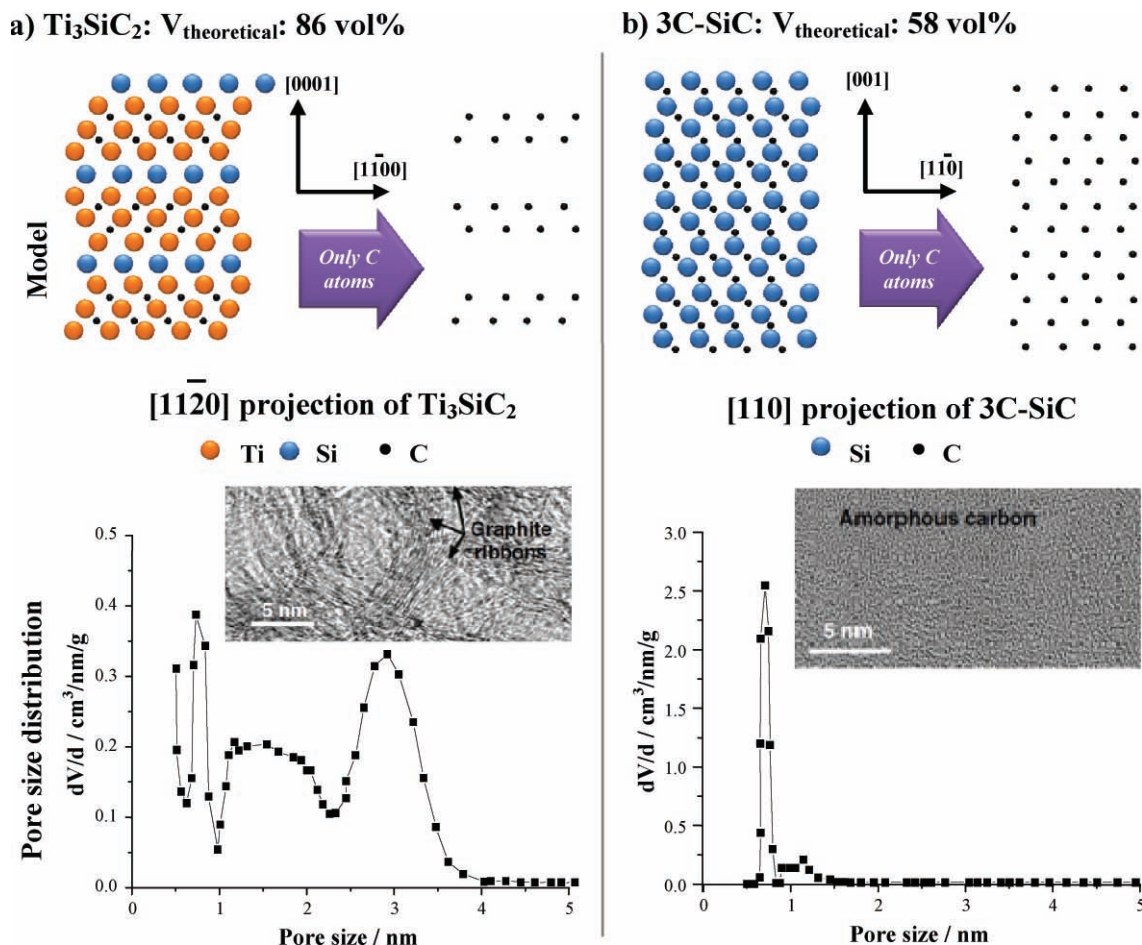


Figure 5. Schematic of the atomic structure of Ti_3SiC_2 (a) and 3C-SiC (b) and the corresponding CDC structures after halogenation. As seen from the pore size distribution, the ternary carbide shows a broader pore size distribution than the binary carbide at $1200\text{ }^\circ\text{C}$. The data are from argon sorption obtained from NLDFT.^[14] Also, we see that for the same chlorination temperature ($1200\text{ }^\circ\text{C}$) the resulting carbon structure can be very different – while SiC CDC still consists of predominantly amorphous carbon, Ti_3SiC_2 CDC shows significant graphitization at the same temperature.^[4,24] Reproduced with permission.^[4] Copyright 2006, CRC Taylor & Francis.

At the same synthesis temperature (e.g., $1200\text{ }^\circ\text{C}$) there is also a large difference in the resulting pore size distribution with a narrow distribution of pore sizes of below 1 nm for 3C-SiC and a broader range of pore sizes of between 0.5 and 4 nm for Ti_3SiC_2 based on gas adsorption data (non-local density functional theory: NLDFT; Ar-sorption). Furthermore, there is a large difference in the ordering of CDC obtained from SiC and Ti_3SiC_2 .

It is possible to calculate the total weight-based theoretical pore volume V_{total} using Equation 4:

$$V_{\text{total}} = \frac{1}{X_{\text{carbon}} \cdot \rho_{\text{carbide}}} - \frac{1}{\rho_{\text{carbon}}} \quad (4)$$

with X_{carbon} being the weight fraction of carbon in the carbide (e.g., for SiC: $X_{\text{carbon}} = 0.30$), ρ_{carbon} the density of carbon (approximated to be 2.2 g cm^{-3} , the density of graphite), and ρ_{carbide} the density of carbide precursor (e.g., TiC: $\rho_{\text{carbide}} = 4.9\text{ g cm}^{-3}$). For silicon carbide, V_{total} is then calculated to be $0.51\text{ cm}^3\text{ g}^{-1}$, which is in agreement with literature.^[39] For

titanium carbide, this yields a net porosity of about $57\text{ vol}\%$ for the CDC. Based on the choice of carbide precursor, we can expect CDC bulk porosity within the range of approximately $50\text{--}90\text{ vol}\%$. Thus, highly porous carbons with open porosity (due to Cl_2/MCl_x transport) can be produced with no additional activation steps.

While the bulk porosity of CDC remains largely unchanged over a wide range of halogenation temperatures, the pore size distribution (PSD) is a function of the temperature. Early studies by Boehm^[37] on CDC formation from TaC and SiC between 500 and $1900\text{ }^\circ\text{C}$ showed characteristic type I N_2 gas adsorption isotherms,^[80] an indication of microporous carbon. This adsorption isotherm type was confirmed for CDC obtained from a large number of carbide precursors and CDC also had a large total specific surface area of up to $2800\text{ m}^2\text{ g}^{-1}$. Mesoporous CDC obtained from polymer-derived ceramics with poly(methylvinyl)silazane as a precursor,^[5] ordered mesoporous carbon produced using a templating approach,^[81] or ordered mesostructured carbide precursors (OM-CDC)^[82,83] show a type IV adsorption isotherm with a characteristic hysteresis loop due

to condensation in the mesopores. For example, Al_4C_3 chlorinated at a low temperature (300°C) was reported to show a type I N_2 adsorption isotherm due to microporous carbon whereas higher temperatures resulted in mesoporous CDC and type IV adsorption.^[46]

Typically, CDCs pore size and PSD are templated by the carbide precursor crystal structure at low temperatures. Carbides with the NaCl structure (e.g., TiC, VC, ZrC) or wurtzite/zinc blend structure (SiC) yield a narrow pore size distribution as the first neighbor separation is uniform (Figure 5b). Rhombohedral B_4C or orthorhombic Mo_2C , with a large and non-uniform nearest neighbor separation, show a wider PSD of the CDC after chlorination.^[39,42,57,84] This uniform nearest neighbor separation is depicted in Figure 5b, where the PSD obtained from Ti_3SiC_2 and SiC precursors are compared at the same synthesis temperature. We can clearly see the trend and the differentiation between intrinsic broad PSD for Ti_3SiC_2 -CDC and narrow PSD for SiC-CDC.

At higher temperatures, there is an increase in pore size due to self-organization and higher carbon mobility along with increased crystallinity of the carbon material.^[85] For many carbide precursors, we find a direct correlation between the halogenation temperature and the resulting pore size with smaller pore sizes at lower temperatures (Figure 6).^[33,46,51,53,86,87] Thus, additional tuning of the pore size is possible by controlling the temperature. Changing the synthesis temperature gives a high level of pore size control with sub-Ångstrom accuracy as shown in Figure 6b, demonstrating why CDC is referred to as a material with tunable porosity.^[86] The pore size distribution displayed in Figure 5b and 6b is even narrower than for single-wall carbon nanotubes.^[4] Broad, yet highly temperature-sensitive pore size distributions can be found for PDC-CDC, as seen in Figure 6c. Yeon et al.^[5] showed that, in PDC SiCN-CDC materials, micropores are formed by etching Si atoms from the SiC phase and mesopores are a result of the elimination of Si-N regions. The resulting hierarchic porosity then strongly

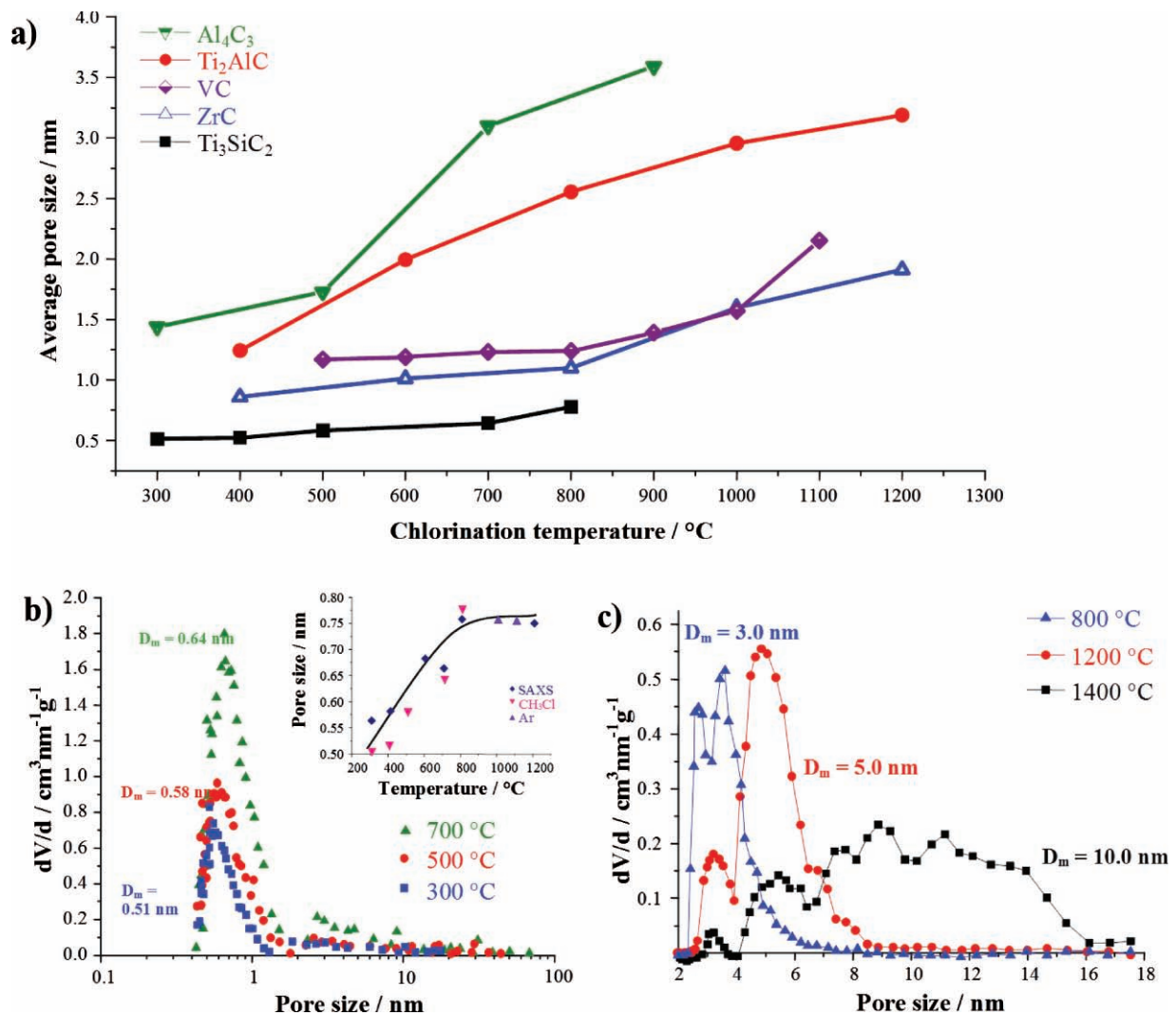


Figure 6. Average pore sizes for selected binary and ternary carbides (a): Al_4C_3 ,^[46] Ti_2AlC ,^[33] VC,^[53] ZrC,^[51] Ti_3SiC_2 .^[86] Comparison between the PSD of Ti_3SiC_2 -CDC^[86] (b) and SiCN PDC-CDC^[5] (c) from nitrogen sorption using NLDFT.

depends on pyrolysis temperature of the pre-ceramic polymer as well as on etching conditions (Figure 6c).

The specific surface area (SSA) changes as a function of ceramic precursor and temperature. For many materials, the SSA was reported to have a bell-shaped temperature dependence.^[42,51] Limiting factors for the SSA include, at low temperatures, clogging of pores with halogenide residues and, at high temperatures, graphitization and CDC consolidation. This explains why there is a maximum SSA at intermediate temperatures of 800–1000 °C.^[42,51] The bell shape is much less pronounced for VC when thorough annealing is performed to remove chlorine-containing residue.^[53] Given that, at low temperatures, pores are templated by the carbide lattice (i.e., pores smaller than 0.5 nm), the corresponding SSA should not decrease but significantly increase. However, such small pores are not accessible for most gas species used for gas adsorption and the resulting values of pore size distribution, total pore volumes, and specific surface area may be underestimated due to the presence of pores smaller than 0.5 nm.

With very high values for the SSA of CDC, it is not clear what the maximum value for a pore volume without additional activation could be. Furthermore, when pore sizes are below 1 nm, smaller than certain molecules, it is better to find the optimal specific surface area for a particular application rather than assume that the SSA measured (e.g., via N₂-gas sorption) would be the same surface area accessible for the sorption of another molecule, e.g., H₂.

3.1.6. Carbon Structure

As discussed before, pore size, PSD, and SSA of the CDC depend on precursor and on halogenation temperatures. The structure of CDC also depends on these parameters. **Figure 7** shows the structural evolution of CDC obtained from chlorination of TiC at different temperatures as a typical example. Starting with highly disordered amorphous carbon, there is a constant increase in structural order with a threshold at around 1000 °C, where the structure becomes dominated by non-planar graphitic carbon. At lower temperatures or shorter chlorination times,^[30] amorphous carbon is found on the surface of carbide particles. With powders (especially nanopowders) we find a higher reactivity due to the higher SSA compared to bulk materials. Consequently, powders react more readily to

form amorphous or disordered porous CDC.^[48] At lower temperatures, such as 600 °C for SiC chlorination, there is no significant increase in the crystallinity of the material. At higher temperatures, graphene sheets and graphite ribbons^[48] with a characteristic d-spacing of <3.4 Å are formed.

Recently, quenched molecular dynamics (QMD)^[88] and reverse Monte Carlo (RMC) simulations^[89] were used to simulate the structure of disordered carbon and the evolution of crystallinity with changing temperature. In agreement with neutron scattering experiments,^[88] modeling showed the same trend of higher short-range order at higher temperatures and an increase in the coordination number (Figure 7).^[88] QMD could be used to reproduce structures that were in morphological agreement with HR-TEM studies of the same material.^[88] At high chlorination temperatures (experimental data; corresponding to slow quench rates for QMD) the structural order that evolves reduces the pores and a corresponding drop in the surface area can be expected. More advanced models, however, are needed to gain a better understanding of disordered porous CDC. They must account for surface termination which will also increase the accuracy of predicting transport in porous carbon networks.

Nanostructures found in CDC obtained from carbide chlorination are more varied than generally depicted in the literature. CDC is often understood and used as a term for amorphous (Figure 1a,b) or highly disordered carbon if produced at a low temperature and increasingly crystalline carbon with evolving graphite ribbons at higher halogenation temperatures (Figure 1b). While amorphous carbon and graphite-like structures form during halogenation, there are many other carbon nanostructures that have been observed for CDC. In fact, transmission electron microscopy (TEM) studies have revealed that different nanostructures such as carbon onions (i.e., concentric spherical graphitic shells), nanodiamond, nanotubes, barrel-like structures and even fullerene-like structures may be found after the chlorination of carbides (Figure 1).

The choice of reaction gas mixture strongly influences CDC formation. Studies on Ar-Cl₂ mixtures revealed that the addition of H₂ to the gas mixture reduced the reaction rate, but at the same time nanodiamond was observed from Raman spectroscopy and electron energy loss (EEL) spectra.^[70,90] In addition to spectroscopy evidence, TEM images^[18,91] of CDC films showed diamond-related lattice fringes, and nanoindentation

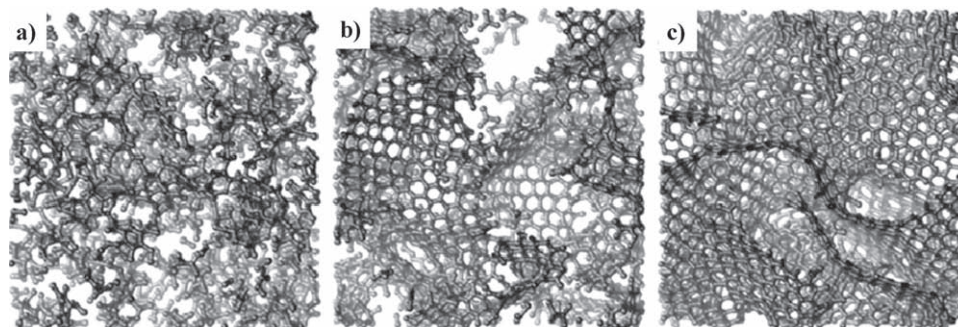


Figure 7. Simulated structure of TiC-CDC obtained after chlorination at 600 °C, which corresponds to fast quenching (A), 800 °C; medium rate (B), and 1200 °C; slow quenching (C).^[88] Reproduced with permission.^[88] Copyright 2010, Elsevier.

studies showed a very high elastic modulus (up to 600 GPa) and high hardness (up to 50 GPa), as expected from diamond-like films.^[90] When a 2.6% Cl₂ : 1.3% H₂ : 96.1% Ar mixture was used at 950 °C,^[70] the hydrogen in the gas mixture favored sp³ bonding by stabilizing dangling bonds formed after the selective halogen removal of silicon from cubic SiC crystals. Local epitaxial nanodiamond growth at the SiC-CDC interface was reported for 1%–3.5% Cl₂ and 0%–2% H₂-Ar at 1000 °C.^[92] CDC coatings obtained from Cl₂:H₂ (2:1) mixtures consisted of a loosely attached, powdery top carbon layer with a dense, highly disordered, adherent, amorphous or nanocrystalline layer below it. The adherent layers were shown to be composed of a mixture of graphitic and diamond-structured carbon^[4] or highly disordered sp² carbon.^[70] The presence of boron and other additives in sintered SiC ceramics may favor diamond formation. It is still not known if sp-bonded carbon can be produced from chlorination of carbide precursors, but modeling suggests the presence of some percentage of 180° bond angles in CDC.^[89]

Nanodiamond formation can also be observed for atmospheres without hydrogen.^[92] In the absence of hydrogen, diamond nanocrystals readily transform to graphitic carbon in the form of curved graphitic structures such as ribbons or onion-like carbon. At low temperatures and limited carbon mobility, nanodiamond formation may be kinetically favored and was observed for various carbides such as SiC, TiC, and ZrC.^[93] Annealing of amorphous CDC after synthesis at moderate temperatures may also lead to the formation of presumably sp³ bonded carbon with a pycnometric density close to that of diamond.^[118] However, the exact mechanism of diamond formation is still unknown and the question remains as to whether nanodiamond can be synthesized as the main component of CDC. The carbon anions in carbide-derived carbon have been reported after chlorination of TiC at 900 °C.^[94] For SiC chlorinated at 1000 °C, both amorphous CDC^[94] and onion-like carbon^[48] were reported in the literature.

Carbon nanotubes were observed in SiC-CDC in 1972.^[95] This may be one of the first observations of nanotubes. CNTs were also later reported for CDC obtained from SiC^[24,34,46,48,90,92,96] Till now, the mechanisms governing the growth of various nanostructures during chlorination of carbides are not yet fully understood. It is clear that the catalytic effect of impurities, additives or the metal of the carbide^[46,97] may play a significant role in nanostructure formation although the low-temperature limit for CDC synthesis and the properties of low-temperature CDC are yet to be determined.

While chlorination temperature and choice of initial carbide are the dominant factors in determining CDC porosity and microstructure, there are also reports on the structural influence of the choice of halogen on the resulting carbon material. CDC obtained from ZrC halogenation in Cl₂, Br₂ and I₂ was studied by Babkin et al.^[28] While similar SSA values were reported for the three different halogens, it was found that ZrC treated by I₂ or Br₂ had the highest sorption capacity for iodine or bromine respectively. This was explained in terms of surface termination and possible effects of the size of the halogen and produced zirconium halogenide molecules. It is important to note that not only porous disordered carbon, but also well-ordered graphite and graphene can be produced by the chlorination of Fe₃C.^[98]

3.1.7. Post-Synthesis Treatment

Another important parameter in tuning the CDC nanostructure is post-synthesis annealing. Usually, a post-synthesis treatment like hydrogenation is carried out after chlorination, at a temperature equal to or lower than the CDC synthesis temperature, to remove residual chlorine or chlorine containing compounds. Considering that up to 40 wt% residual chlorine was captured in the pores after Ti₃SiC₂ chlorination and cooling in chlorine flow, it is obvious that chlorine removal via post-synthesis treatment is important for CDC.^[24] Post-synthesis annealing opens up clogged pores and results in larger measured specific surface areas.^[44] It is important to choose post-synthesis annealing conditions in such a way that beneficial properties like the high SSA are not compromised. Compared to treatment with ammonia or hydrogen, argon annealing shows limited potential in chlorine removal.^[36] In particular, ammonia treatment yielded the lowest residual chlorine concentration especially for CDC obtained at temperatures below 1000 °C. The high reactivity of CDC with ammonia was corroborated in a recent study by Adu et al.^[99]

The importance of annealing conditions is also reflected in the carbon structure, where an initially disordered CDC structure is largely maintained during argon annealing while a higher degree of structural order can be observed after NH₃ or H₂ annealing at the same temperature.^[36] It is important to note that the resulting properties such as excess uptake of gas for gas storage may be affected by post-treatment procedures. H₂ annealing, for instance, was reported to improve hydrogen storage capacity.^[100] Both gases, H₂ and NH₃, can chemically react with chlorine leading to HCl formation. The latter can be easily removed from pores because of its smaller molecular diameter.

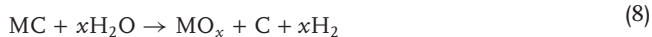
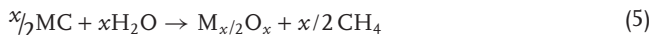
Apart from treatment in H₂ or NH₃, other reactive procedures have been reported to improve the properties of CDC. Mixtures of 90 wt% TiC with 10 wt% TiO₂ were used for chlorination instead of pure TiC.^[101] TiO₂ in the chlorine atmosphere was used to controllably oxidize some of the created CDC and additional modification of the pore structure was obtained by adjusting the temperature or by controlling the CO–CO₂ equilibrium. As a result, pore coarsening was observed (0.8 nm compared to 0.6–0.7 nm for pure TiC). Similarly, a water/argon mixture annealing at 900 °C^[102,103] or water vapor etching^[104] resulted in larger surface area, and pore coarsening.

3.2. Hydrothermal Treatment

3.2.1. Basics of the Hydrothermal Decomposition of Carbides

Hydrothermal treatment is another way for reactive chemical removal of metal or metalloid atom(s) from the carbide network to produce CDC. Carbon formation by hydrothermal treatment was first reported in the early 1990s for amorphous Si-Ti-C-O (Tyranno) fibers.^[105,106] The term hydrothermal refers to hot, high-pressure (usually supercritical) water at typical temperatures in the range of 200–1000 °C and pressures of up to hundreds of MPa. Studies were later expanded to pure silicon carbide fibers^[12,107,108] and bulk materials.^[109]

Thermodynamic calculations for a number of metal carbides under hydrothermal conditions were carried out using Gibbs energy minimization algorithms. Jacobson studied a wide temperature (300–1000 °C) and pressure range (2–200 MPa) for M_xC-H_2O with $M = Si, Ti, Ta, Nb, W$ or B .^[110] The thermodynamic analysis indicated that carbon, MO_x , CH_4 , CO_2 , CO , and H_2 are the main products of hydrothermal reactions in the temperature range of the study, and the principal reactions were written as follows:



Thermodynamically speaking, the formation of an oxide phase indicates the formation of both carbon and metal oxide, and from kinetic considerations, supercritical water can be a potent solvent, especially for silica. Data on the solubility of SiO_2 strongly depends on the chosen pressure, temperature and pH conditions, and values are as low as several nm per year at temperatures below 100 °C and at a pH of 7.^[71] At 285 °C and 100 MPa, a silica solubility rate of $2.5 \cdot 10^{-8} \mu m s^{-1}$ can be expected in distilled water^[111] and by increasing the temperature to 500 °C, solubility rate increases to several $\mu m s^{-1}$.^[112] For other metal oxides, we do not expect such high dissolution rates, but rather the formation of oxides and hydroxides that are mixed with carbon in the final reaction product.

Experimental studies on SiC clearly demonstrated that carbon formation is sensitive to the water-to-carbide ratio, and three different stoichiometry-governed regimes were identified.^[113,114] At low $H_2O:SiC$ ratios, both carbon and silica are deposited on the surface. At intermediate $H_2O:SiC$ ratios, carbon and silica are formed but the large surplus of water ensures that any formed silica is immediately dissolved into the fluid and carbon remains the only stable solid reaction product. Finally, at higher $H_2O:SiC$ ratios, neither carbon nor silica is formed and only active oxidation of silicon carbide is observed.

A critical factor for the carbon yield is the amount of carbon-containing gas species formed during hydrothermal decomposition of the carbide precursor. As a temperature-sensitive factor, the yield of CH_4 decreases with increasing temperature as CH_4 is unstable at high temperatures, resulting in an increase in the amount of carbon produced.^[113] Higher pressures, on the other hand, increase the stability of methane leading to a lower carbon yield. From calculations, we expect that TaC, TiC, and NbC should show a behavior very similar to that of SiC although we must account for a lower metal oxide solubility in hydrothermal fluids for most oxides. Boron carbide, however, was predicted not to yield any carbon under hydrothermal conditions.^[113]

3.2.2. Carbon Structure

Raman spectra of CDC produced by hydrothermal treatment on Tyranno fibers (amorphous SiO_xC_y with nanometer-sized β -SiC) showed a band of graphite (G) and a disorder-induced band (D), confirming the formation of amorphous/disordered graphitic carbon.^[115] However, the carbon film was porous and provided no protection against further reaction, exactly as in the case of chlorination.^[116]

Formation of amorphous carbon after hydrothermal treatment was reported on the surface of Tyranno fibers at 300–400 °C and 100 MPa^[107,108] CVD-SiC fibers after treatment at 400–700 °C and 200 MPa,^[117] and α - and β -SiC platelets, whiskers, and powders at 600–800 °C.^[110,118,119] Diamond-structured carbon, graphite, and amorphous carbon were found on the surface of α - and β -SiC powder and single crystals after treatment at 300–800 °C and 100–500 MPa.^[120,121] Experimental data confirms carbon formation via hydrothermal treatment for WC, TaC, NbC, and TiC at 500–750 °C and 100–170 MPa.^[120] With ternary carbides, one must consider the formation and possible dissolution kinetics of at least two metal oxide species. In the case of Ti_3SiC_2 , rutile/anatase along with highly disordered carbon was reported after hydrothermal treatment at 35 MPa for temperatures ranging between 500 and 700 °C.^[122] The presence of sp^2 and sp^3 hybridized carbon was confirmed via X-ray photoelectron spectroscopy (XPS), and Raman data suggests that at higher temperatures a smaller domain size can be found, as indicated by an increased I_D/I_G ratio.^[122]

In the presence of organic acids such as malonic acids or sucrose, SiC was reported to decompose, producing silica and either glassy carbon or carbon nanospheres.^[123] Spherical and filamentous carbon were also reported for these acidic organic materials in the hydrothermal decomposition of chromium carbide (Cr_3C_2).^[124] When exposed to a hydrothermal environment alone, Cr_3C_2 showed either no reaction at low temperatures (<300 °C) or only the formation of chromium oxide at higher temperatures (>350 °C).^[124] It should be noted that hydrothermal decomposition of organic compounds like polyethylene yields various carbon nanostructures, such as carbon nanotubes.^[125]

3.3. Thermal Decomposition of Carbides

3.3.1. General Aspects of Thermal Decomposition

Thermal decomposition in a vacuum or in high-temperature inert atmospheres is another route to transform carbides into carbon due to incongruent melting of carbide and evaporation of the carbide-forming elements, as the melting point of carbon exceeds that of most metals.^[126] Most studies have concentrated on the thermal decomposition of silicon carbide in various forms (powder, fibers, single crystals, wafers etc.) mainly because silicon carbide is not only the most common carbide but is currently the only carbide for which large single crystals are commercially available. The potential of vacuum decomposition to synthesize high-purity epitaxial graphitic carbon was also demonstrated for Al_4C_3 by Foster et al.^[127]

Similarly to the discussion in Section 2.1.3, one should consider that once formed, silicon must be transported outward through the inward growing carbon layer.^[47] For short diffusion path lengths, we observe effectively linear decomposition kinetics. As the porous carbon film forms, a gradient in the Si vapor pressure builds up within that layer through which all further decomposed silicon must diffuse through. Once Si vapor reaches the surface of the carbon layer, it effuses away from the material into the environment since effusion is faster than the diffusion of Si through carbon. Si transport is presumably the rate controlling step. There is indirect evidence of silicon surface migration during the silicon carbide decomposition in studies by Voronin et al.^[128,129]

First studies of SiC decomposition were carried out in the late 1940s^[130,131] where dense graphitic carbon was found after heating to 2000 °C.^[132] Early experiments by Badami showed that heating 6H-SiC single crystals to 2050–2150 °C at 10⁻⁵ Torr, yields turbostratic carbon and graphitic carbon that exhibits epitaxial features with respect to the underlying SiC lattice. In fact, it was observed that carbon layers are ordered either parallel or perpendicular to the SiC stacking direction (i.e., *c*-axis). Within the turbostratic carbon matrix, graphite crystals with a common *c*-axis to the SiC substrate were identified with an outer layer dominated by turbostratic carbon and the graphite domains close to the SiC-C interface.^[133] Electron beam induced carbon formation on 6H-SiC also strongly indicated topotaxial CDC with graphite layers parallel to the basal plane of silicon carbide.^[134] Interestingly, studies on β -SiC whiskers thermally decomposed at 2400 °C and 10⁻⁶ Torr yielded graphite nanocrystallites with no epitaxial relation to the carbide precursor lattice.^[135] This was attributed to the size effect and lack of exposed basal planes. Additionally, it was observed that the basal planes of the graphite domains were tangent to the whisker surface.^[135]

A critical aspect to carbon formation from SiC was addressed by Badami: the number of carbon atoms in a layer of SiC is smaller than required for forming a dense graphite layer. In fact, one graphene layer consumes 2–3 SiC bilayers.^[136] Structural reorganization is, therefore, a key parameter of carbide decomposition and it is facilitated by higher carbon mobility at elevated temperatures.^[137] Structural reorganization especially applies to the complexity of initial carbon formation and its interplay with surface reconstruction of silicon carbide. Presently, 800 °C marks the lower temperature limit for carbon formation via thermal decomposition,^[137] but it may depend on SiC surface conditions as temperatures higher than 1100 °C are typically reported.^[135]

With silicon carbide itself being extremely complex with more than 280 different polytypes,^[138] surface reconstruction of SiC^[71,138] is beyond the scope of this paper. It is, however, essential to consider the SiC polytype when discussing the initial stages of carbon formation and especially the forming of single-layer graphene, where the interaction between the carbon layer and the underlying SiC layer is important. Another key aspect of carbon formation from SiC is the well-known anisotropy which is reflected in almost all physical and chemical properties of silicon carbide. As a result; we see different carbon nanostructures and growth rates for the different SiC surfaces as reflected by the large difference in surface energy of

2.2 J m⁻² for the Si-face and 0.3 J m⁻² for the C-face.^[139] Carbon growth on the C-face was reported to be as much as five times faster than on the opposing Si-face.^[140]

Surface inhomogeneities such as scratches also play a vital role in what and where carbon nanostructures of different types are formed. Cambaz et al.^[6] reported enhanced carbon formation around scratches on the carbide surface as defects and strained Si-C bonds accelerate thermal decomposition. Impurities, such as sodium, were also reported to give rise to the formation of non-planar graphitic carbon on the surface of silicon carbide single crystals. Both scratches and impurities weaken the influence of the protective oxide layer on silicon carbide, which shields the substrate from vacuum decomposition. The role of the initial oxide layer, with thicker scales on the Si-face and thinner layers on the C-face, should always be taken into account.^[141]

3.3.2. Conservation of Shape

In 1962, Badami pointed out that vacuum decomposition of SiC conserves the original carbide shape so that even nanoscopic features such as growth steps are visible in the resulting CDC.^[136] In similarity with the shape conservation of SiC fibers transformed into CDC by chlorination shown in Figure 4, we observed a conservation of the shape of β -SiC whiskers annealed in vacuum (10⁻⁵ Torr) at 1700–2000 °C.^[30] However, some sharp edges were smoothed after vacuum decomposition at higher temperatures as a result of the higher carbon mobility and graphite formation. Iijima^[134] observed a minor loss of the original particle shape after electron-beam assisted vacuum decomposition of SiC while the SiC-C interface was still topotaxial. Cambaz et al.^[6] showed that scratches on the SiC surface remaining after polishing were still visible on the CDC surface after vacuum decomposition, demonstrating the shape conservation during carbon formation (Figure 8a).

3.3.3. Carbon Nanotubes Produced by SiC Decomposition

In 1997, Kusunoki et al. demonstrated that vacuum decomposition of silicon carbide can be used to epitaxially produce self-organized carpets of carbon nanotubes.^[11] A typical CNT film on SiC is shown in Figure 8a.^[6] One important feature of CNT grown via SiC decomposition is that no metal catalyst is involved in any step of nucleation or growth of the films.^[11,142–145] The resulting CNT films are reported to consist of carbon nanotubes of the same chirality^[142,143] while other methods, such as laser evaporation or CVD, usually result in zigzag, armchair, and chiral tubes coexisting in the products.^[2]

First experiments reported by Kusunoki et al.^[11] were performed on β -SiC single crystals that were rapidly heated to 1700 °C at 10⁻⁹ Torr using in situ laser heating in a TEM.^[146] Overlapped CNTs with caps of 2–5 nm oriented along the [111] direction on (111)- β -SiC single crystal were observed after heat treatment. Similar results were obtained from heating SiC in a vacuum furnace, giving rise to continuous CNT films.^[144] Kusunoki et al.^[11] and Shimizu et al.^[147] reported that β -SiC (111) CVD films on Si were transformed into freestanding CNT films by SiC decomposition and subsequent removal of the SiO₂/Si substrate.

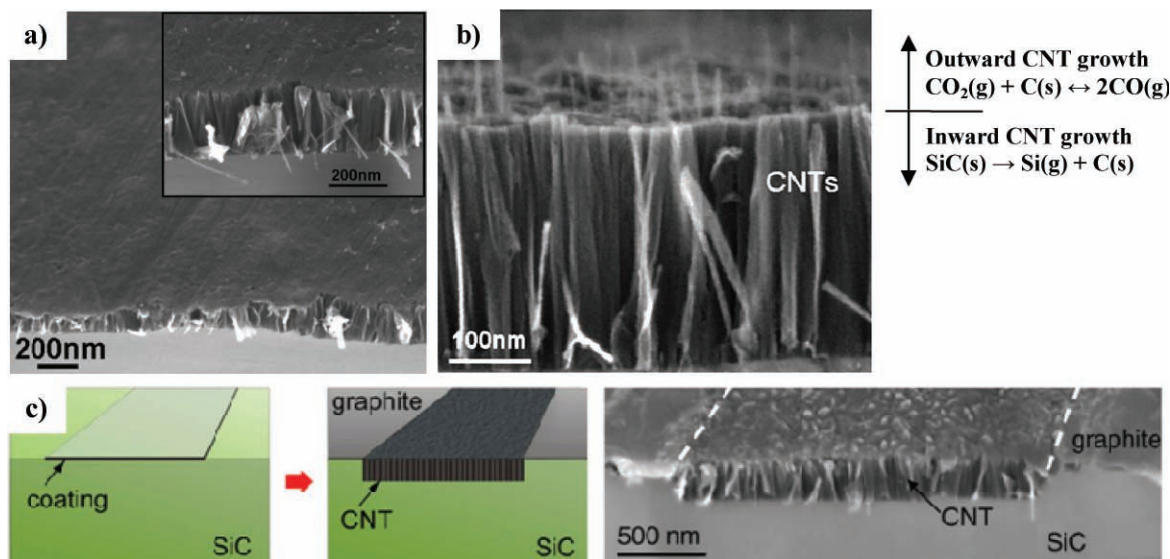


Figure 8. SEM images of different carbon nanostructures obtained from vacuum decomposition of 6H-SiC for the C-face in high vacuum (a) and Si-face in low vacuum (b), respectively.^[6] The SEM image shows an example of the carbon film with conformal transition where the initial scratches from sample polishing are still evident and dense CNT brushes as obtained. Outward growth of CNT is facilitated by the Boudouard reaction. Surface modification (c) is capable of triggering or suppressing CNT growth, thus enabling surface patterning. Reproduced with permission.^[6] Copyright 2008, Elsevier.

Critical factors to consider when forming CNT films are the crystallographic orientation of the free SiC surface, surface quality (defects, impurities), crystal morphology and the decomposition conditions (vacuum, temperature). The spectrum of obtained tubes ranges from MWCNT (multi-wall carbon nanotubes) for SiC powder^[148] to double/triple wall CNT for SiC wafers^[11,142–146] and defect-rich SWCNT (single-wall carbon nanotubes) for SiC nanopowders.^[149]

A model for CNT formation from SiC was proposed by Kusunoki et al.^[8,11,142–145] The model suggests residual oxygen as the driving force of CNT formation. At temperatures at or below 1000 °C, graphite sheets are formed on free-standing silicon carbide surfaces by oxidative extraction of silicon from the SiC crystal lattice, and no CNTs are observed in this regime. Temperatures near 1300 °C are accompanied by bubble formation due to emerging SiO gas that can no longer diffuse through the formed carbon film fast enough to avoid uplifting the carbon film. As a result, so called carbon nanocaps formed which continued to grow as carbon nanotubes for longer times and/or higher decomposition temperatures.

Carbon nanocap formation was observed for 3C-SiC in an in situ study and an onset of nanocap formation of 1360 °C was observed at 3×10^{-7} Torr.^[150] In the same study, it was shown that amorphous carbon is formed at the initial stage which then transforms epitaxially into graphene sheets. In a final stage at temperatures above 1500 °C, enhanced CNT growth was observed.^[144] A higher temperature limit for CNT growth seems to be around 1900 °C. As found by Cambaz et al.,^[6] the C-face of 6H-SiC vacuum decomposed at 10^{-6} Torr at 1800 °C showed predominantly curved and planar graphite walls with individual nanotubes normal to the surface.

Significant differences in the carbon structures were identified when comparing the Si- and the C-face of 6H-SiC.^[142,145] While CNT growth was observed under various experimental

conditions on the C-face, mainly flat graphite sheets parallel to the surface alone were found on the Si-face.

Nagano et al.^[151] observed CNTs growing perpendicular to the Si-face after HF etching. These CNT were less than half the length and larger in diameter than the CNT on the C-face. The effect of HF etching leading to surface reconstruction was discussed as the reason for Si-face CNT growth by Wang et al.^[152] An initial oxide layer on any SiC surface prevents CNT growth as Si–O bonds need to be broken and oxygen needs to be removed from the surface before carbon nanotubes can be formed.^[151]

Recent quantum chemical molecular dynamics simulations show that nanocap formation on the C-face can be explained as the result of the two opposing forces of C–C σ -bond formation and persistence of π conjugated graphene sheets^[140,152] independent of SiO-related formation mechanisms. This results in repulsion between carbon atoms at the center of nanocaps which later grow to become CNTs. Removal of Si from the Si-face leads to the growth of a flat graphene layer underneath the evaporating Si-layer which continues to grow as a stack of planar graphitic sheets.^[152] These simulations also provided an explanation for the zigzag-like chirality of the C-face grown CNTs, as a consequence of a 90° angle between the silicon carbide surface and unsaturated sp^3 bonds.^[140]

While lower temperatures (<1500 °C) yield graphitic carbon layers, higher temperatures show CNT formation on the C-face.^[144] It should be noted that CNT films were reported for lower temperatures starting around 1250–1300 °C by Kusunoki.^[144] It was also shown that it is possible to obtain both CNT formation on the Si-face and enhance CNT growth on the C-face by addition of CO₂.^[6] This illustrates that gas transport plays an important role in CNT formation and growth. Therefore, tubes grown in presence of CO (CO₂ reaction with carbon) are longer and protrude from the source (Figure 8b), since additional carbon is supplied through the gas phase.

The Kusunoki model^[144] does not explain the differences in C- and Si-face but only the transition from graphite to CNT. Explanations for SiC anisotropy mainly consider the thickness and composition of the initial oxide layer and the quality of the polished surface, but do not consider different bonding configurations^[153,154] and different growth kinetics.^[3] It has been shown that, by surface modification, both CNT and graphite can be grown on both C- and Si-faces of SiC enabling surface patterning (Figure 8c).^[6]

Similarly, different carbon nanostructures were observed on the C-face of SiC.^[144] While most graphite (0002) planes are perpendicular towards (0001)-6H-SiC (Figure 9a), it can be

seen that, along a step, the graphite basal planes remain perpendicular to the original carbide surface toptotaxially instead of epitaxially. The lower part left of the step now shows (0002) graphite that is oriented parallel to (0001)-6H-SiC. Amorphous carbon forms on amorphized SiC surfaces (Si- and C-faces alike) instead of graphitic carbon/CNT.^[155]

CNT layers as obtained from thermal decomposition of 6H-SiC wafers at 1700 °C were reported to show high elastic modulus (17–20 GPa) viscoelastic behavior and a very high resistance to buckling.^[158] The latter is a direct consequence of the high packing density of vertically standing MWCNTs (2–4 walls) giving raise to pronounced viscoelastic behavior due to Van der

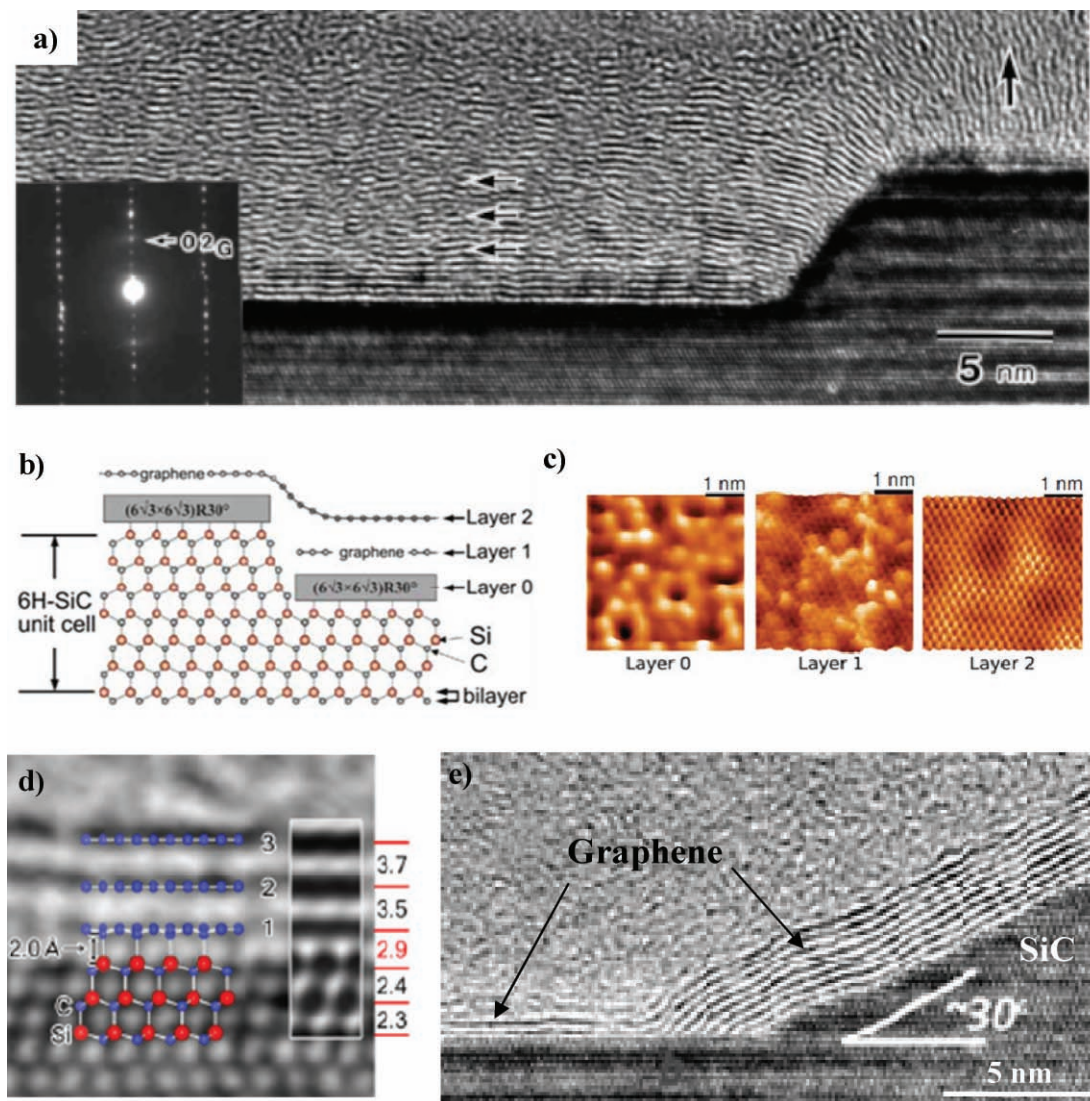


Figure 9. Influence of surface morphology on topotaxial carbon formation (a).^[144] Schematic illustration of graphene growth on the Si-face of 6H-SiC (b, Ref. [156]). After forming a buffer layer (layer 0) graphene layers emerge with characteristic nanostructure. Scanning tunnel microscopy shows the characteristic, well-ordered honeycomb arrangement of carbon atoms in layer 2 (c).^[156] From the HR-TEM image (d) we can see that the bonding distance between the first graphene layer and the topmost SiC layer is significantly smaller than the graphene–graphene spacing yet larger than the SiC bilayer distance.^[7] A different number of graphene layers (e) can be seen on a 30° terrace step (110n).^[157] Reproduced with permission.^[144] Copyright 1999, Taylor & Francis. Reproduced with permission.^[156] Copyright 2010, Materials Research Society. Reproduced with permission.^[7] Copyright 2009, Elsevier.

Waals interactions between the tubes. These CNTs could be used for applications where mechanical energy must be absorbed. CNT films obtained from catalytic synthesis have already demonstrated their potential as electrical brush contacts.^[159]

However, it is still unclear how to grow SWCNT arrays via extraction of silicon from the SiC precursor. Also, systematic studies of CNT growth on carbides other than SiC are missing and may provide new insights into the CNT growth mechanism.

3.3.4. Graphene Formation by SiC Decomposition

Graphene is the product of SiC vacuum decomposition^[160,161] or heating in inert gas atmospheres.^[8,162] Described by van Bommel in 1975,^[160] it was referred to as a monocrystalline or thin graphite layer before the term graphene was introduced in 1987.^[163] From the CNT growth model, it is assumed that a thin graphene layer forms prior to CNT uplift. To avoid any bubble formation, graphene formation from SiC requires stable vacuum conditions (e.g., 10^{-5} – 10^{-10} Torr,^[157,164] inert atmospheres at ambient pressure, or extremely low oxygen partial pressures^[5,8,162] With the limitations of exfoliation, epitaxial graphene on SiC is a promising way to obtain homogenous films on a large scale.^[156,165] On an atomic level, however, SiC is not perfectly flat but characterized by steps and terraces that play an important role in graphene growth.

A detailed description of the graphene formation model can be found in References 165 and 166. Nucleation was reported to start at the terrace steps that equal the (110 n) face of SiC.^[7,157] The initial stage of graphene layer formation at terrace steps is characterized by step bunching of two SiC bilayers as a result of preferential decomposition on edges. Hupalo reported that three terrace steps can recede to give rise to one graphene layer.^[166] Step erosion was linked to the differences in the surface energy of (0001) vs. (110 n) SiC and the high number of dangling bonds at (110 n) SiC.^[8,166,167] As step erosion continues, continuous graphene films form, promoted by enhanced carbon mobility at high temperatures. Pit formation is commonly observed during SiC decomposition at temperatures below 1200 °C^[168] and is associated with point defects rather than dislocations.^[169] It must be considered as a detrimental effect as it locally distorts the uniformity of the graphene layer.^[156,170,171] Terraces also show a different number of graphene layers as in the basal plane depicted in Figure 9e.^[157]

From a structural point of view, one should consider epitaxial aspects of graphene growth (Figure 9) as well as topotaxial effects. For the Si-face, SiC first reconstructs^[156] to form a $(6\sqrt{3}\times 6\sqrt{3})R30^\circ$ so called “buffer” layer (layer 0 in Figure 9)^[172,173] with a carbon density close to that of monolayer graphene^[170] and close interactions with the SiC substrate as shown by a band gap.^[174] Layer 1 will then be formed on top of the buffer layer. The buffer layer provides some isolation from the substrate by saturating dangling bonds, giving rise to the well-known honeycomb-like structure and electric conductivity found in layer 1. This is seen from the scanning tunnel microscopy (STM) images presented in Figure 9c. Also, layer 0 is much closer to the SiC surface (2.9 Å) in comparison to the graphene-graphene interlayer distance (~3.5 Å). Subsequent graphene layers, like layer 2 in Figure 9d, will then be formed as the SiC decomposition progresses.

Control of graphene growth is important because graphene multilayers show a decay of performance,^[175] such as reduced electron mobility, with an increasing number of layers, approaching the properties of bulk graphite at a threshold of circa 10 layers, as known from ab initio calculations.^[176] Thus, one should adjust the heating rate or time/temperature to minimize excess carbon formation during heating and choose suitable annealing conditions.

The C-face of SiC shows graphene that is, however, often distorted by nanocaps, the onset of nanotube formation, or rotational carbon domains.^[140] Therefore, the Si-face that has a slower growth rate and allows a better control over the number of layers is usually used for graphene growth.^[157] Thicker carbon layers are also likely to show wrinkles.^[6,168,177]

In reported studies on graphene formation from SiC vacuum decomposition, conditions vary from no sample polishing,^[166] to Si-deposited SiC surfaces^[178,179] and hydrogen etched silicon carbide.^[164,173] The topmost layer of SiC must be critically considered when looking at the formation of graphene single layers. Optimal graphene growth will only be observed for atomically flat and defect free surfaces. The latter may only be possible to a certain degree but it is clear that regular chemical mechanical polishing (CMP) may not be sufficient. There are several reports on different procedures for SiC surface treatment.^[180–185] Etching SiC wafers prior to synthesis is a possible route to remove surface defects.^[169,184] Hydrogen etching at 1500 °C yielded step heights of approximately 15 Å,^[184] which is equal to the unit cell length of 6H-SiC.^[186]

Also, substrate orientation is important; it was reported^[187] that reducing the off-axis deviation for the (0001) plane from the c -axis from 0.25° to 0.03° significantly reduces terraces on the polished SiC. Instead of a 2 µm terrace width and 40–50 Å step height, improved characteristics (width: 6 µm; height: 10–15 Å) are a result of better control of the crystal orientation of the carbide surface. Below that threshold of approximately 10–15 Å, there seem to be fundamental limitations to obtain atomically flat surfaces.

Graphene formation was described for doped (n- and p-type) and semi-insulating silicon carbide.^[6,174,188] In a recent study by Yang et al.,^[189] different nitrogen doping levels were investigated and it was shown that the charge carrier type and concentration of epitaxial graphene can be controlled by the substrate. Graphene growth from other carbide precursors, possibly even at temperatures below the graphene growth onset level for silicon carbide, has not been studied in detail yet. Work in this area is necessary to improve our basic understanding of graphene formation and its relation to the carbide substrate it originates from. Formation of well-ordered graphite/graphene by chlorination of Fe₃C has been shown,^[98] suggesting that graphene growth on carbides may be achieved in various environments.

4. Examples of Applications of CDC

Given the variety of CDC nanostructures, it is obvious that there are numerous potential applications. CDC, in particular, is a powerful selective sorbent for various molecules^[3] and is suitable for applications such as purification of noble gases^[190] or removal of toxins and cytokines from human blood.^[55] The

removal of toxic compounds from water or capacitive water desalination are other fields of possible application for carbide-derived carbon. There is a large variety of further applications for CDC such as; as catalyst supports for fuel cells,^[191] as supercapacitor electrodes,^[9] as electrodes for Li-air and Li-ion batteries, or for hydrogen and methane storage.^[74] Electrical energy storage and gas storage are only two of many examples, although they are currently the most extensively studied ones. In the next sections, a few selected applications are highlighted in more detail.

4.1. Electrode Material for Supercapacitors and Li-ion Batteries

Capacitive energy storage has recently attracted much attention because of fast energy uptake (in seconds) and delivery with an efficiency of more than 95%.^[9,192] Unlike batteries, where energy is stored chemically, supercapacitors or electric double-layer capacitors (EDLC) use physical charge separation on high surface area electrodes, making the process of charging and discharging fast and completely reversible. In fact, more than a million recharge cycles and an expected service lifetime of more than 10 years have been reported for commercial supercapacitors. Even after 20 years, a capacity degradation of only 50% was reported for commercially available supercapacitors.^[9,193] Typical applications can be found in the field of personal electronics, mobile telecommunications, back-up power storage and boosters for vehicles.^[194] As a more recent example, the Airbus A380 employs supercapacitors for its 16-door emergency door opening system.^[9]

CDC with controllable nanostructure and pore characteristics, obtained by chlorination of various ceramic precursors such as TiC,^[41,56,195–198] SiC,^[56,199] Ti₂AlC,^[54,56] B₄C,^[29,54] Al₄C₃,^[56,58] Mo₂C,^[56,84] or VC,^[200] have been studied as supercapacitor electrode materials. Differences in total pore volume, pore size distribution and carbon structure of CDC prepared from various carbide materials are also reflected in the capacitance.^[201] Gravimetric capacitance of 190 and 150 F/g was found for ZrC-CDC and TiC-CDC, respectively, in H₂SO₄.^[50] In KOH electrolyte, Al₄C₃-derived carbon showed a higher gravimetric capacitance (260 F/g) than SiC-CDC (200 F/g) and TiC-CDC performs better in organic electrolytes such as TEA-BF₄-ACN (tetraethylammonium-tetrafluoroborate in acetonitrile; 140 F/g)^[202] than CDC from B₄C (75 F/g) or SiC (110–120 F/g).^[61] It has also been shown that capacitance of CDC decreases with increasing particle size.^[78,81,199]

Mesoporous Mo₂C-derived CDC also yielded a high gravimetric capacitance of 143 F g⁻¹ in 1 M (C₂H₅)₃CH₃NBF₄ electrolyte in acetonitrile,^[84] while VC-CDC showed a capacitance of 133 F g⁻¹ in the same organic electrolyte.^[200] Up to 180 F g⁻¹ capacitance in organic electrolyte has been reported for KOH activated TiC-CDC by Portet et al. and explained by a significantly increased specific surface area.^[198]

While the carbide precursor, particle size and other parameters affect CDC capacitance, the synthesis temperature has the most significant impact on the capacitance of CDC, because it affects the pore size (Figure 6a). Tunability of pore size in CDC facilitated a major breakthrough in understanding capacitive charge storage in porous carbon. Chmiola et al. reported

an increase in the gravimetric and volumetric capacitance at lower chlorination temperatures, although the specific surface area and pore size of CDC decreased.^[202] Traditionally, a decrease in capacitance was expected for submicrometer pores that are inaccessible to the electrolyte.^[203] Studies performed on CDC with 0.7 to 1.1 nm pores^[202] have shown that for small pores, the solvation shell of the electrolyte ions is completely or partially removed leading to an increase in the capacitance. A later study on the correlation between pore size and capacitance corroborated an increase in capacitance when the pore size approaches that of the desolvated ion and a decrease once the pore size is smaller than the ion size.^[204] The importance of pore size tuning with sub-Angström accuracy was shown on an example of an ionic liquid electrolyte (Figure 10).^[205] A similar bell-shaped curve was described by Thomberg et al.^[200] for a 1 M (C₂H₅)₃CH₃NBF₄ acetonitrile solution, where VC-CDC obtained by chlorination at 900°C, and with pores of an average diameter of 1.18 nm, gave the highest capacitance value of 133 F/g. Thus, the tunability of CDC pore size (Figure 6a) and controlled PSD allows optimization of electrodes for a variety of electrolytes which is difficult to achieve using other carbons.

Templated mesoporous carbon is another material exhibiting high capacitance. Korenblit et al. showed that nanostructured silicon carbide obtained from a mesoporous silica template yields CDC with a capacitance of up to 170 F g⁻¹ for 1 M TEA-BF₄ solution in acetonitrile.^[81] A high total surface area, pore sizes tuned to the electrolyte ion size, and ensuring that all pore volume is accessible to ions without transport limitations is the key for achieving high capacitance.

Different approaches for the manufacturing of CDC electrodes have been proposed. Usually, CDC powder is mixed with a binder material such as polytetrafluorethylene (PTFE) or polyvinylidene fluoride (PVDF) and then formed into a 100–200 micrometer thick film in the same way as activated carbon.^[50,53,56,84,200,206,207] The use of materials without polymer binders may increase electrical conductivity and CDC/pyrolytic carbon composites offered an increased mechanical strength,^[208,209] but only up to 39 F/cm³ capacitance, as reported in aqueous electrolytes for these materials.^[210]

It should be noted that in a binder/CDC mixture or any other powder-based electrode, there will be a significant interparticle macropore volume filled with electrolyte that cannot be used for capacitive energy storage. Thus, monolithic microporous bodies are another approach to improve device performance.^[41] As illustrated in Figure 11, and compared with other carbon materials, the volumetric capacitance can be significantly increased for monolithic CDC films. A maximum value of 180 F/cm³ for TiC-CDC was reported in a recent study for 2 μm thick thin films in 1.5 M TEA-BF₄-ACN, and of 160 F cm⁻³ in aqueous electrolyte.^[41] Lower values of below ~30 F cm⁻³ were found in organic electrolyte for thick films of over 100 μm due to limitations in ion transport.^[41] CDC films can be created on a large number of different substrate materials.^[63] This enables the direct manufacturing of supercapacitors with high volumetric capacitance on a silicon chip.^[41,63] An example of a TiC-CDC thin film with enhanced volumetric capacitance is shown in Figure 11b.

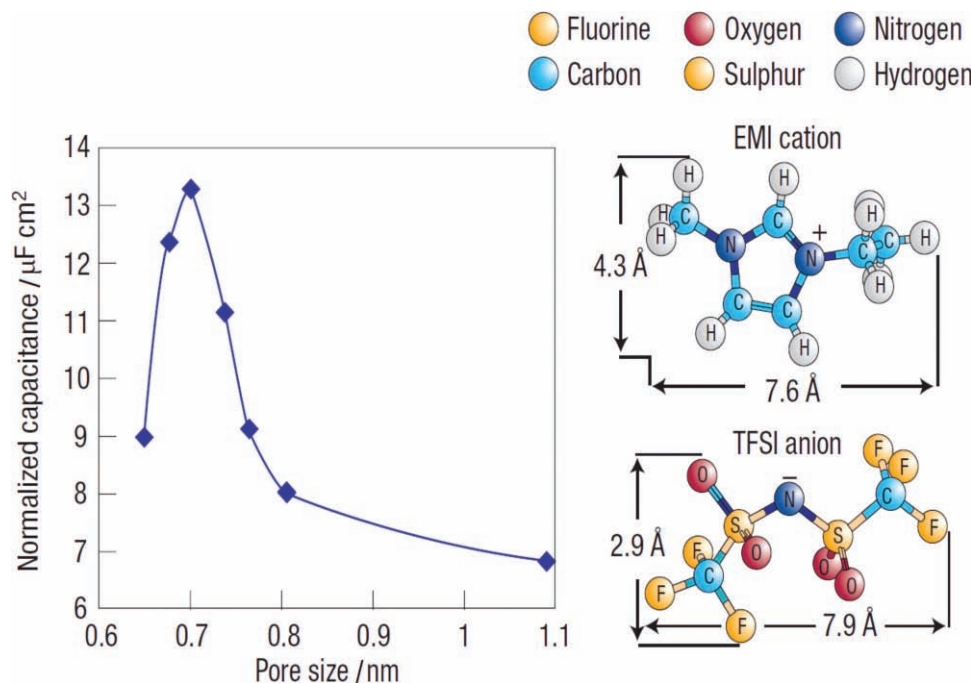


Figure 10. Correlation between capacitance in EMI-TFSI ionic liquid electrolyte (normalized by SSA) and TiC-CDC pore size.^[205] Reproduced with permission.^[205] Copyright 2008, American Chemical Society.

The use of CDC as electrode material in anodes of lithium-ion batteries has also been explored. When SiC-, TiC- and Mo₂C-derived CDCs^[211] were lithiated between 30 °C and 200 °C, LiC₁₂ and LiC₂₄ were identified via XRD in addition to LiC₆.^[212,213] Li₂CO₃ and Li₂C₂, which are detrimental to capacitance, were present to a lesser amount. Based on diffusion data,^[213] lithium ion diffusion occurs mainly along pore walls and Li accumulates in the pores forming metal clusters. Disordered carbons in general and CDC in particular may offer a longer life cycle and faster charge/discharge rates in comparison to graphite, which requires Li ions to intercalate between the closely-spaced graphene layers, leading to slower charge-discharge rates and faster material degradation. This material degradation, for example, has been seen in a recent patent on the use of CDC materials from a variety of carbide precursors for lithium battery electrode materials.^[214]

4.2. Graphene-based Electronic Devices

Because of extraordinary properties like the 100-fold increase in the intrinsic carrier mobility (both electron and hole mobility) at room temperature in comparison with silicon, graphene transistors have attracted much attention lately.^[215–218]

It was demonstrated that working graphene microdevices can be built using exfoliated graphene.^[219,220] Novoselov et al.^[219] reported on device sizes up to 10 μm. However, the reproducible manufacturing of devices for real-world applications requires a well-controlled process. Vacuum decomposition of SiC wafers yields uniform graphene layers which are convenient for

micropatterning^[164] using electron beam lithography or conventional etching.^[217,218] Li et al.^[221] showed that millimeter-sized top- and side-gated graphene field effect transistors can be made from graphene epitaxially grown by vacuum decomposition of silicon carbide. Both Si and C-face 6H-SiC were studied for graphene transistors, and graphene on the Si-face of 6H-SiC was reported to have a higher off-to-on resistance ratio but a much smaller carrier density compared to the C-face.^[221] Anisotropic transport properties of epitaxial graphene field-emission transistors (FETs) are associated with faceting of SiC and can be observed for (110n) steps.^[222] This is associated with different properties of graphene on basal plane and (110n) SiC.

As long as graphene is attached to SiC, it will not necessarily show the same properties as exfoliated and suspended graphene. It was found, for example, that the electron mobility in graphene on SiC is lower by an order of magnitude than that of exfoliated graphene, as a consequence on the interaction between graphene and the carbide substrate. There is a similar decrease for supported exfoliated graphene due to long-range scattering.^[165,223] Epitaxial graphene on SiC can be removed from the substrate via the so called Scotch tape method.

Another application of graphene is in electrodes of supercapacitors.^[224] It has been shown by Stoller et al.^[224] that a sufficiently high gravimetric capacitance can be achieved from agglomerated graphene produced from graphite oxide in aqueous (99 F/g) and organic (135 F/g) electrolytes. Similarly to CDC^[41,63] or carbon onions,^[225] graphene nanosheets can be used in micro-supercapacitors, providing a very short response time.^[226] Future research will explore CDC-based graphene in current collectors and in the electrodes of high power micro-supercapacitors with high charge/discharge rates.

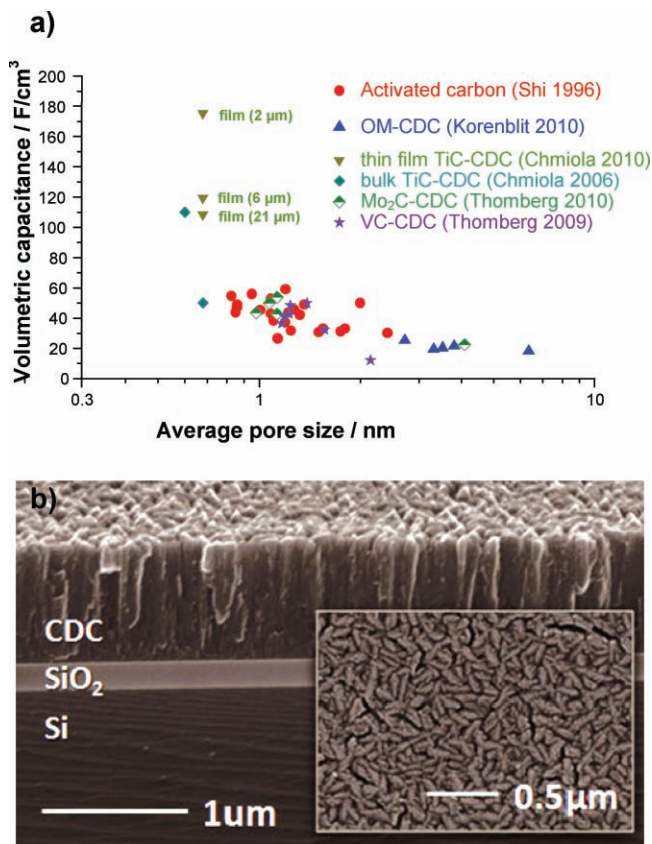


Figure 11. Volumetric capacitance vs. average pore size in 1.5 M TAE-BF₄-ACN (after Fernandez et al.,^[201] Shi,^[203] Korenblit,^[81] Chmiola 2010,^[41] Chmiola 2006,^[202] Thomberg 2010,^[84] Thomberg 2009^[200]) for CDC powders and films of different thickness (a). Example of a CDC film with enhanced volumetric capacitance (TiC-CDC thin film on a Si wafer with thermally grown SiO₂ layer) (b). Reproduced with permission.^[63] Copyright 2010, RSC Publishing.

4.3. Gas Storage (Hydrogen, Methane)

Reversible gas storage is of critical importance in fuel cells and other technologies. Storage of liquid hydrogen requires cryogenic cooling, and compressed hydrogen storage is less efficient in terms of required storage container volumes when compared to hydrocarbon storage. Therefore, materials which show a high physisorption capacity at moderate temperatures are essential for a more efficient storage of gases such as hydrogen or methane.

CDC can be optimized to adsorb a large quantity of methane. Gogotsi^[227] reported a sorption capacity of 40 cm³/g at ambient pressure and temperature for SiC-CDC chlorinated at 1200 °C, whereas B₄C-derived CDC only shows 10 cm³ g⁻¹ under the same conditions. CDC outperforms commercially available activated carbons, offering 2.8 wt% methane storage at ambient temperature and pressure. Post-synthesis activation in CO₂ or KOH significantly improves the gravimetric methane uptake from TiC-CDC as shown by Yeon et al.^[228] The best excess gravimetric methane uptake of 18.5 wt% at 25 °C and 60 bar (16 wt% at 35 bar) was obtained with a TiC-CDC activated with CO₂ at 975 °C for 2 h, yielding material with a surface area of 3360 m² g⁻¹.^[228,229]

Without activation, TiC-CDC shows values of ~14 wt% excess methane uptake at 35 bar and 25 °C (Figure 12a).^[74] Bulk TiC-CDC plates showing an excess uptake of 21 wt% were reported. However, since bulk CDC has no macroporosity, this translates to a very high volumetric uptake compared to CDC powder.^[74]

The hydrogen storage capacity of CDC has also been studied.^[227] Early studies by Gordeev et al. showed that hydrogen can be chemisorbed on SiC-CDC at 300–600 °C with efficient desorption at 400–1200 °C.^[208,209] A later study characterized the hydrogen uptake for SiC- and Al₄C₃-CDC.^[190] A total hydrogen uptake at 1 MPa at 27 °C of 0.5 wt%, 1 wt% at –78 °C and 2 wt% at –196 °C was reported.

Yushin et al.^[100] studied the pore size effect on hydrogen uptake at cryogenic temperatures by using CDC from various carbide precursors (TiC, ZrC, B₄C and SiC). The best results were obtained for hydrogen-annealed TiC-CDC; a gravimetric H₂ uptake of up to 3 wt% and volumetric density of 24 kg m⁻³ was identified at 1 atm and –196 °C. Direct comparison of the H₂ uptake between TiC-CDC with and without subsequent hydrogen annealing showed that post-synthesis H₂ annealing increases the sorption capacity of CDC by 75%. When average pore diameter is below 1 nm, there is a linear correlation between the pore volume and the H₂ uptake.^[100] KOH activation is also a suitable method to obtain a larger gravimetric H₂ storage; at –196 °C and 20 bar, an increase of H₂ uptake of 63% compared to as-synthesized ZrC-CDC was demonstrated.^[52] At –196 °C and 1 atm, KOH-activated ZrC-CDC shows less H₂ uptake than as-produced TiC-CDC. Monolithic TiC-CDC was reported to show improved gravimetric hydrogen storage capacity compared to powders (Figure 12c, d).^[74]

4.4. Tribological Coatings

Many carbide materials are used in sliding contact applications because of their high wear resistance, strength and chemical stability. To decrease their friction coefficient, especially during dry friction, a carbon coating can be used on SiC. The SiC surface is transformed into carbon by inward growth of the adherent CDC layer giving rise to a tight, well defined SiC/C interface.^[38,62,75] Chlorination at 700–1000 °C was used to form a CDC layer on sintered SiC ceramics and was shown to effectively reduce the friction coefficient from >0.7 for SiC to <0.2 under dry running conditions^[230] as shown in Figure 13.^[231]

Even lower friction coefficients of <0.1 in dry nitrogen were observed after annealing CDC in Ar + 5% H₂ at 800 °C.^[230] This behavior is unlike that of graphite and other sp² carbons, where the presence of water vapors is required for lubricity and durability. The tribological properties of CDC in both wet atmospheres and dry environments were explained by the presence of carbon onions, water adsorption in CDC micropores, and termination of dangling carbon bonds with hydrogen.^[230] The 3-dimensional carbon network of CDC (Figure 7) provided sufficient mechanical strength and a kind of “ductility” (inset in Figure 13) that prevents brittle fracture and allows “smoothing” of the CDC film surface during friction.

CDC coatings were also used to enable pull-out and increase damage tolerance in composite materials applied on SiC fibers.^[69] They could also function as a sacrificial layer for the

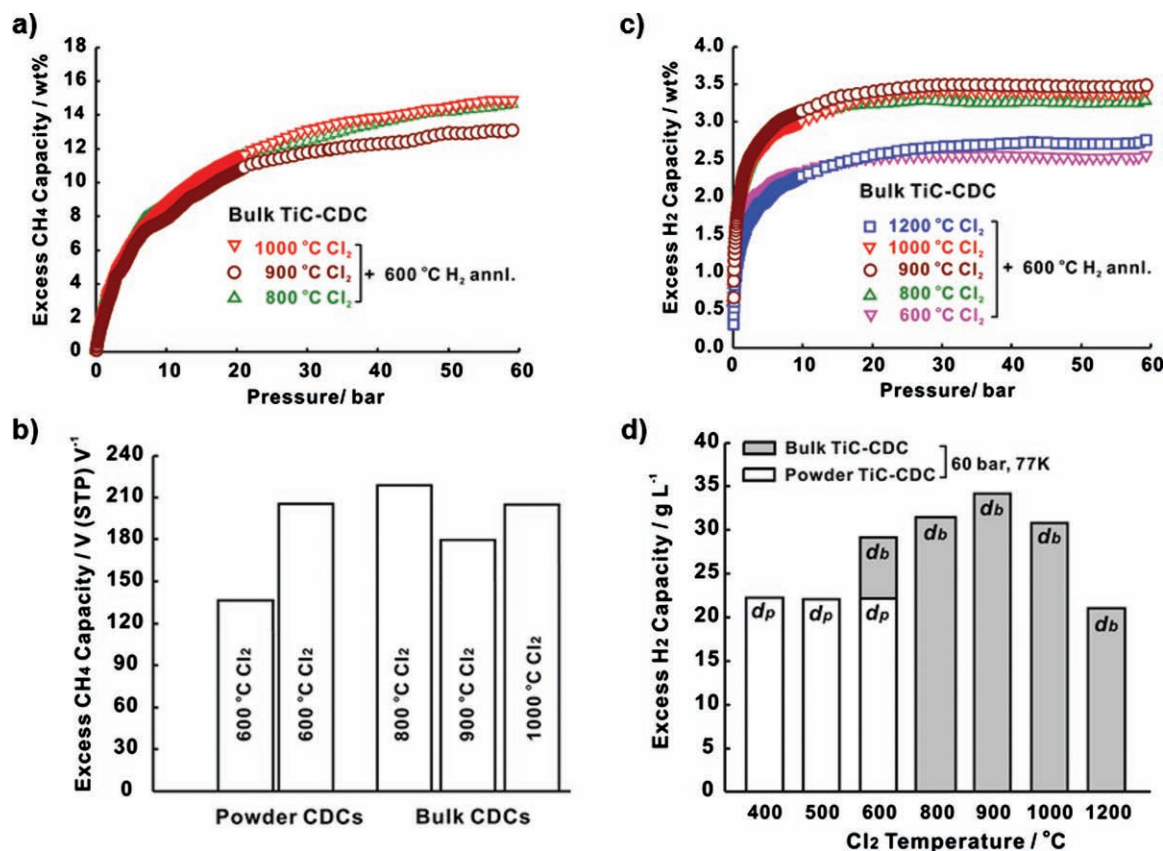


Figure 12. Excess methane (26 °C) (a) and hydrogen (−196 °C) (b) adsorption isotherms along with volumetric excess methane (c) and hydrogen (d) uptake.^[74] It is evident that bulk TiC-CDC shows a much higher volumetric gas storage capacity than powder. Reproduced with permission.^[74] Copyright 2010, Elsevier.

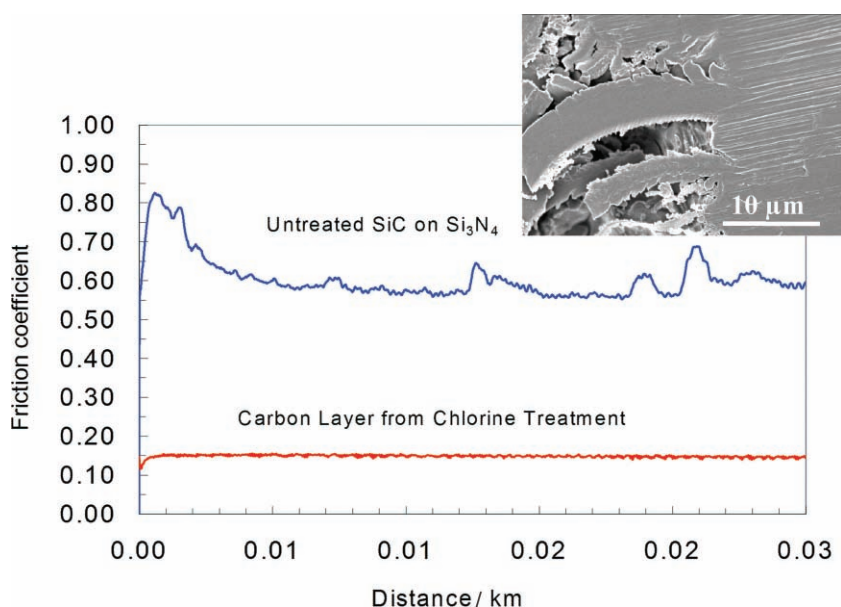


Figure 13. Impact of CDC coating on the dry friction coefficient of SiC. As seen, a decrease of factor 4 for the friction coefficient was observed. The inset shows a SEM image of the worn surface and plastic extrusion of the carbon coating into a pore.^[231] Reproduced with permission.^[231] Copyright 2000, Taylor & Francis.

formation of BN or Al-O-N coatings, as both are known to show superior oxidation resistance.^[232–233] Synthesis of a sacrificial layer comprises several steps. First, CDC is formed via chlorination gas treatment at ambient pressure and elevated temperatures. As a second step, B₂O₃ (for BN) or 0.15 M ethyl ether solution of AlCl₃ (for Al-O-N) is infiltrated in the porous CDC at room temperature and subsequently annealed in NH₃ to form a nitride coating. Due to the conformal carbide–CDC transition, this process is suitable for producing BN or Al-O-N based coatings with a smooth surface and excellent bonding to the residual SiC fiber core.^[234] As a result, >65% higher tensile strength values and a threefold increase in the Weibull modulus was reported for CDC coated fibers compared to uncoated SiC fibers.^[233]

4.5. Pt Catalyst on CDC Support

Pt/C catalysts supported on SiC-CDC were reported in several studies^[234] and were

introduced either by a conventional wet chemical route with subsequent annealing to control the Pt particle in the nanometers range size, or directly during CDC synthesis. During SiC chlorination, metallic platinum was introduced into the reaction zone and effectively dispersed in the produced material by transport toward the SiC/C interface as gaseous Pt_3Cl_3 that reacts with SiC to form Pt and SiCl_4 , forming layers of platinum particles.^[234] As the carbon nanostructure is barely affected by the additional presence of platinum, only small molecules can penetrate into the film and reach Pt particles embedded in the CDC structure. An example for such a Pt/C composite is displayed in **Figure 14**.^[234] It can be clearly seen that the resulting material shows Pt layers which is an interesting structure of potential interest for catalyst applications. Besides Pt, other well-dispersed metal nanoparticles can be introduced into CDC.^[235]

4.6. Protein Sorption

CDC shows pore-size dependent sorption of ions and molecules and this property can be used for the purification of biofluids, especially given that CDC, as with most other carbons, has good biocompatibility.^[55,236] While micropores are needed for supercapacitors and gas storage, sorption of biomolecules, which have sizes of several nanometers, requires mesoporous materials with a high surface area. Mesoporosity is expected to yield a much higher sorption capacity compared to microporosity because of the larger surface area accessible to protein molecules.^[55] CDC derived from Ti_2AlC and Ti_3AlC_2 by chlorination at 600–1200 °C was subjected to annealing in argon, ammonia, hydrogen, chlorine and vacuum.^[236] Fast removal of inflammatory cytokines such as TNF- α , IL-6, and IL-1 β , which is necessary to stop the progression of sepsis, was demonstrated. It was most efficient for NH_3 annealed ternary carbide CDC, because the positively charged aminated surface attracts negatively charged protein molecules. In particular, mesoporous Ti_2AlC -derived carbon obtained by chlorination and annealing

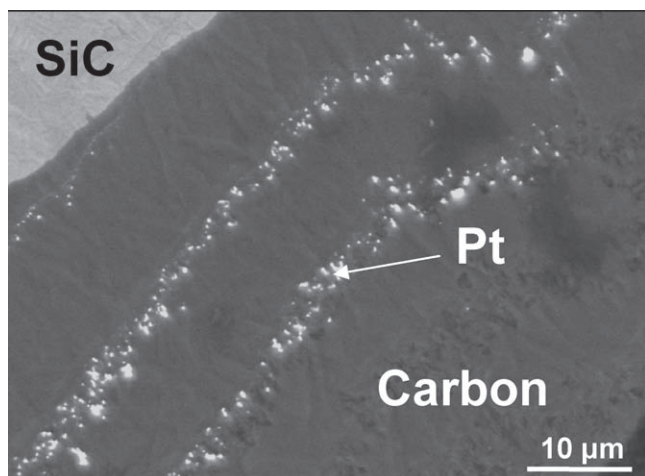


Figure 14. SEM image of a layered Pt-carbon film produced by chlorination of SiC in presence of platinum.^[234] Reproduced with permission.^[234] Copyright 2001, The Electrochemical Society.

in NH_3 at 800 °C yielded complete removal of the large cytokine TNF- α from blood plasma in less than an hour, with >85% and >95% TNF- α removal in 5 and 30 min, respectively. Compared to activated carbons,^[55] this is a significant improvement and shows that CDC offers promise as a sorbent for a variety of biomolecules.

5. Conclusions

Carbide-derived carbons include a large group of materials ranging from fully amorphous to highly ordered structures that can be produced by extracting metals or metalloids from carbides using halogens, supercritical water, selective oxidation, vacuum decomposition and other chemistries. Starting as an undesired by-product of SiCl_4 synthesis,^[21] CDC has evolved from a novel amorphous carbon^[15] to a designer carbon material.^[4] Virtually any known carbon structure—graphene, nanotubes, diamond, or porous amorphous networks—can be synthesized by this method. The important milestones in CDC development were the observation of CNT formation^[11] and graphene growth^[160] during thermal decomposition of silicon carbide, as well as discovery of the tunability of the pore size.^[86] The ability to control the pore size and pore size distribution by varying chlorination temperature^[86] and choice of carbide precursors led to development of a large family of porous carbons.^[237]

With a large number of different structures and a wide range of properties, CDC is being evaluated for a variety of applications. CDC is now one of the most researched materials for supercapacitor electrodes^[1,9] because its tunable pore size allows optimization of porosity for any electrolyte. The tunability of pore size of CDC can be used to optimize the carbon for selective molecule sorption and water purification. Much potential also lies in gas storage where CDC shows high volumetric sorption capacity for hydrogen and methane and also for CO_2 , Cl_2 , and many other gases used in energy or chemical technology. The excellent tribological properties of CDC coatings have found applications in dynamic seals. Applications of CDC in Li-batteries sensors, electronic devices and on-chip power sources are being explored. Mesoporous CDC with the pore size templated by the carbide precursor and well-determined surface chemistry has demonstrated its potential in adsorbing cytokines from blood plasma.

The cornerstone of all current and future applications of CDC will always be a comprehensive understanding of the relationship between carbide structure, carbon synthesis conditions, post-synthesis treatment and the resulting CDC structure and properties. This explains why current research focuses on controlling the nature of the carbide precursors – either by using polymer-derived ceramics (PDC-CDC) or by creating ordered mesoporous carbide as a starting material for CDC synthesis (OM-CDC). For the latter, processes such as electrospinning can be applied.^[72] Also, templates such as biomimetic TiC obtained by chemical treatment of carbonized paper, have been investigated.^[79] The latter processes produce CDC fabric or fibers that can be used for advanced engineering applications.

Acknowledgements

The authors thank the US Department of Energy (award numbers ER46473, DE-FGOI-05ER05-01), US National Science Foundation (award numbers ICC-0924570, DMR-0945230), and the Army Research Office for funding and Y-Carbon for providing samples for our research. YG and VP were supported as part of the Fluid Interface Reactions, Structures and Transport (FIRST) Center, an Energy Frontier Research Center funded by the U.S. Department of Energy, Office of Science, Office of Basic Energy Sciences under award no. ERKCC61. VP acknowledges the financial support from the Alexander von Humboldt Foundation. YG would also like to thank his current and former students and post-docs, especially, Dr. J. Chmiola, Dr. R.K. Dash, Dr. G. Yushin, Dr. S.-H. Yeon and Dr. C. Portet for experimental help, as well as collaborators Prof. J.E. Fischer, Prof. P. Simon, Prof. M.J. McNallan, Prof. M. Barsoum, Prof. M. Yoshimura, and Prof. B. Etzold for helpful discussions. We are thankful to R. Swartz, D. Tadros, and J. McDonough for comments on the manuscript.

Received: October 5, 2010

Published online: February 9, 2011

- [1] F. Beguin, E. Frackowiak, *Carbons for Electrochemical Energy Storage and Conversion Systems*, CRC Press, Boca Raton, FL **2009**.
- [2] Y. Gogotsi, *Carbon Nanomaterials*, CRC Taylor & Francis, Boca Raton **2006**
- [3] A. Nikitin, Y. Gogotsi, in *Encyclopedia of Nanoscience and Nanotechnology*, Vol. 7 (Ed: H. S. Nalwa), American Scientific Publishers, Valencia, CA **2004**, 553.
- [4] G. Yushin, A. Nikitin, Y. Gogotsi, in *Carbon Nanomaterials*, (Ed: Y. Gogotsi), CRC Taylor & Francis, Boca Raton FL **2006**, 211
- [5] S.-H. Yeon, P. Reddington, Y. Gogotsi, J. E. Fischer, C. Vakifahmetoglu, P. Colombo, *Carbon* **2010**, *48*, 201.
- [6] Z. G. Cambaz, G. Yushin, S. Osswald, Y. Mochalin, Y. Gogotsi, *Carbon* **2008**, *46*, 841.
- [7] W. Norimatsu, M. Kusunoki, *Chem. Phys. Lett.* **2009**, *468*, 52.
- [8] K. Emtsev, A. Bostwick, K. Horn, J. Jobst, G. Kellogg, L. Ley, J. McChensney, T. Ohta, S. Reshanov, J. Röhr, E. Rotenger, A. K. Schmid, D. Waldmann, H. B. Weber, T. Seyller, *Nat. Mater.* **2009**, *8*, 203.
- [9] P. Simon, Y. Gogotsi, *Nat. Mater.* **2008**, *7*, 845.
- [10] C. Berger, Z. M. Song, X. B. Li, X. S. Wu, N. Brown, C. Naud, D. Mayou, T. B. Li, J. Hass, A. N. Marchenkov, *Science* **2006**, *312*, 1191.
- [11] M. Kusunoki, M. Rokkaku, T. Suzuki, *Appl. Phys. Lett.* **1997**, *71*, 2620
- [12] Y. G. Gogotsi, K. G. Nickel, P. Kofstad, *J. Mater. Chem.* **1995**, *5*, 2313
- [13] N. F. Fedorov, *Russ. J. Inorg. Chem.* **1995**, *39*, 73.
- [14] T. Kyotani, J. Chmiola, Y. Gogotsi, in *Carbon Materials for Electrochemical Energy Storage Systems*, (Eds: F. Beguin, E. Frackowiak), CRC Press/Taylor and Francis, Boca Raton, FL **2009**, 77.
- [15] W. A. Mohun, in *Proceedings of the Conference on Carbon*, Vol. 4, **1959**, 443.
- [16] G. Yushin, R. Dash, J. Jagiello, J. Fischer, Y. Gogotsi, *Adv. Funct. Mater.* **2006**, *16*, 2288.
- [17] J. S. Bae, T. X. Nguyen, S. K. Bhatia, *J. Phys. Chem. C* **2010**, *114*, 1046.
- [18] T. X. Nguyen, J. S. Bae, S. K. Bhatia, *Langmuir* **2009**, *25*, 2121
- [19] P. Krawiec, E. Kockrick, L. Borchardt, D. Geiger, A. Corma, S. Kaskel, *J. Phys. Chem. C* **2009**, *113*, 7755.
- [20] P. Krawiec, D. Geiger, S. Kaskel, *Chem. Comm.* **2006**, *23*, 2469
- [21] O. Hutchins, *US Patent 1271713*, **1918**.
- [22] J. N. Andersen, *US Patent 2739041*, **1956**.
- [23] G. F. Kirillova, G. A. Meerson, A. N. Zelikman, *Izvestiya Vuzov, Tsvetnaya, Metallurgiya* **1960**, *3*, 90.
- [24] G. N. Yushin, E. N. Hoffman, A. Nikitin, H. Ye, M. W. Barsoum, Y. Gogotsi, *Carbon* **2005**, *43*, 2075.
- [25] V. P. Orekhov, G. V. Seryakov, A. N. Zelikman, T. M. Starobina, T. I. Kahzanova, K. V. Petrova, P. M. Sverchkov, *Zh. Prikl. Khim.* **1969**, *42*, 230.
- [26] A. K. Kuriakose, J. L. Margrave, *J. Phys. Chem.* **1964**, *68*, 2343.
- [27] A. K. Kuriakose, J. L. Margrave, *J. Phys. Chem.* **1964**, *68*, 290.
- [28] O. E. Babkin, G. K. Ivakhnyuk, N. F. Fedorov, *Zh. Prikl. Kh.* **1983**, *57*, 504.
- [29] H. Wang, Q. Gao, *Carbon* **2009**, *47*, 820.
- [30] Z. G. Cambaz, G. N. Yushin, Y. Gogotsi, K. L. Vyshnyakova, L. N. Peresentseva, *J. Am. Ceram. Soc.* **2006**, *89*, 509.
- [31] W. C. Schumb, J. R. Aronson, *J. Am. Chem. Soc.* **1959**, *81*, 806.
- [32] N. Batisse, K. Guerin, M. Dubois, A. Hamwi, L. Spinelle, E. Tomasella, *Thin Solid Films* **2010**, *518*, 6746.
- [33] E. N. Hoffman, G. Yushin, T. El-Raghy, Y. Gogotsi, M. W. Barsoum, *Microporous Mesoporous Mater.* **2008**, *112*, 526.
- [34] E. N. Hoffman, G. Yushin, M. W. Barsoum, Y. Gogotsi, *Chem. Mater.* **2005**, *17*, 2317.
- [35] G. K. Ivakhnyuk, O. E. Babkin, N. F. Fedorov, *Zh. Fiz. Khim.* **1993**, *67*, 2052.
- [36] C. Portet, D. Kazachkin, S. Osswald, Y. Gogotsi, E. Borguet, *Thermochim. Acta* **2010**, *497*, 137.
- [37] H. P. Boehm, H. H. Warnecke, in *Proc. 12th Biennial Conf. on Carbon*, Pergamon, Oxford **1975**, 149.
- [38] A. Erdemir, A. Kovalchenko, M. J. McNallan, S. Welz, A. Lee, Y. Gogotsi, B. Carroll, *Surf. Coat. Technol.* **2004**, *188–189*, 588.
- [39] N. F. Fedorov, G. K. Ivakhnyuk, D. N. Gavrilov, *Zh. Prikl. Khim* **1982**, *55*, 243.
- [40] S. Urbonaite, S. Wachtmeister, C. Mirguet, E. Coronel, W. Y. Zou, S. Csillag, G. Stevansson, *Carbon* **2007**, *45*, 2047.
- [41] J. Chmiola, C. Largeot, P. L. Taberna, P. Simon, Y. Gogotsi, *Science* **2010**, *328*, 480.
- [42] R. K. Dash, A. Nikitin, Y. Gogotsi, *Microporous Mesoporous Mater.* **2004**, *72*, 203.
- [43] N. F. Fedorov, G. K. Ivakhnyuk, D. N. Gavrilov, *Zh. Prikl. Khim* **1982**, *55*, 40.
- [44] G. Laudisio, R. K. Dash, J. P. Singer, G. Yushin, Y. Gogotsi, J. E. Fischer, *Langmuir* **2006**, *22*, 8945.
- [45] A. Lee, R. Y. Zhu, M. McNallan, *J. Phys.: Condens. Matter* **2006**, *18*, S1763.
- [46] J. Leis, A. Perkson, M. Arulepp, M. Käärik, G. Svensson, *Carbon* **2001**, *39*, 2043.
- [47] K. Motzfeldt, M. Steinmo, in *Proceedings of the 9th International Conference on High Temperature Materials Chem.*, Vol. 97–39 (Ed: K. E. Spear), The Electrochemical Soc., Inc., Pennington, NJ **1997**, 523.
- [48] S. Welz, M. J. McNallan, Y. Gogotsi, *J. Mater. Process. Technology* **2006**, *179*, 11.
- [49] A. N. Zelikman, L. M. Leonova, *Tsvetn. Met.* **1978**, *19*, 54.
- [50] J. Chmiola, G. Yushin, R. Dash, Y. Gogotsi, *J. Power Sources* **2006**, *158*, 765.
- [51] R. K. Dash, G. Yushin, Y. Gogotsi, *Microporous Mesoporous Mater.* **2005**, *86*, 50.
- [52] M. Sevilla, R. Foulston, R. Mokaya, *Energy Environ. Sci.* **2010**, *3*, 223.
- [53] A. Jänes, T. Thomberg, E. Lust, *Carbon* **2007**, *45*, 2717.
- [54] J. Chmiola, G. Yushin, R. K. Dash, E. N. Hoffman, J. E. Fischer, M. W. Barsoum, Y. Gogotsi, *Electrochem. Solid-State Lett.* **2005**, *8*, A357.
- [55] G. Yushin, E. N. Hoffman, M. W. Barsoum, Y. Gogotsi, C. A. Howell, S. R. Sandeman, G. J. Phillips, A. W. Lloyd, S. V. Mikhailovsky, *Biomaterials* **2006**, *27*, 5755.

- [56] A. Jänes, L. Permann, M. Arulepp, E. Lust, *Electrochem. Comm.* **2004**, *6*, 313.
- [57] A. E. Kravchik, J. A. Kukushkina, V. V. Sokolov, G. F. Tereshchenko, *Carbon* **2006**, *44*, 3263.
- [58] M. Lätt, M. Käärik, L. Permann, H. Kuura, M. Arulepp, J. Leis, *J. Solid State Electrochem.* **2010**, *14*, 543.
- [59] D. Avila-Brandé, E. Urones-Garrote, N. A. Katcho, E. Lomba, A. Gomez-Herrero, A. R. Landa-Canovas, L. C. Otero-Diaz, *Micron* **2007**, *38*, 335.
- [60] E. Urones-Garrote, D. Avila-Brandé, N. Ayape-Katcho, A. Gomez-Herrero, A. R. Landa-Canovas, L. C. Otero-Diaz, *Carbon* **2005**, *43*, 978.
- [61] Y. Xiong, Y. Xie, X. Li, Z. Li, *Carbon* **2004**, *42*, 1447.
- [62] M. McNallan, D. Ersoy, R. Zhu, A. Lee, C. White, S. Welz, Y. Gogotsi, A. Erdemir, A. Kovalchenko, *Tsinghua Sci. Technol.* **2005**, *10*, 699.
- [63] M. Heon, S. Lofland, J. Applegate, R. Nolte, E. Cortes, J. D. Hettinger, P.-L. Taberna, P. Simon, P. Huang, M. Brunet, *Eng. & Environ. Sci.* **2011**, *4*, 135.
- [64] D. Hobgood, M. Brady, W. Brixius, G. Fechko, R. Glass, D. Henshall, J. Jenny, R. Leonard, D. Malta, S. G. Müller, V. Tsvetkov, C. Carter, Jr., *Mater. Sci. Forum* **2000**, 338–342, 3.
- [65] J. Tang, J. S. Zabinski, J. E. Bultman, *Surf. Coat. Technol.* **1997**, *91*, 69.
- [66] T.-H. Wang, A. M. Navarette-Lopez, S. Li, D. A. Dixon, *J. Phys. Chem. A* **2010**, *114*, 7561.
- [67] Y. G. Gogotsi, I.-D. Jeon, M. J. McNallan, *J. Mater. Chem.* **1997**, *7*, 1841.
- [68] P. F. Becker, F. Glenk, M. Kormann, N. Popovska, B. J. M. Etzold, *Chem. Eng. J.* **2010**, *159*, 236.
- [69] L. Chen, G. Behlau, Y. Gogotsi, M. J. McNallan, *Ceram. Eng. Sci. Proc.* **2003**, *24*, 57.
- [70] D. A. Ersoy, M. J. McNallan, Y. G. Gogotsi, *Mater. Res. Innovations* **2001**, *5*, 55.
- [71] V. Presser, K. G. Nickel, *Crit. Rev. Solid State Mater. Sci.* **2008**, *33*, 1.
- [72] M. Rose, E. Kockrick, I. Senkovska, S. Kaskel, *Carbon* **2010**, *48*, 403.
- [73] J. A. H. da Jornada, S. Block, G. J. Piermarini, *Appl. Phys. Lett.* **1984**, *45*, 700.
- [74] S.-H. Yeon, I. Knoke, Y. Gogotsi, J. E. Fischer, *Microporous Mesoporous Mater.* **2010**, *131*, 423.
- [75] D. A. Ersoy, M. J. McNallan, Y. Gogotsi, in *Proc. Electrochem. Soc.* **1998**, 98–99, 324.
- [76] F. J. Norton, *Nature* **1961**, *191*, 701.
- [77] W. Pabst, E. Gregorova, *J. Mater. Sci.* **2004**, *39*, 3501.
- [78] N. Popovska, M. Kormann, *JOM J. Min. Met. Mater. Soc.* **2010**, *62*, 44.
- [79] M. Kormann, H. Gerhard, N. Popovska, *Carbon* **2009**, *47*, 242.
- [80] K. S. W. Sing, *Pure Appl. Chem.* **1985**, *57*, 603.
- [81] Y. Korenblit, M. Rose, E. Kockrick, L. Borchardt, A. Kvit, S. Kaskel, G. Yushin, *ACS Nano* **2010**, *4*, 1337.
- [82] G. Cheng, D. H. Long, X. J. Liu, L. C. Ling, *New Carbon Mater.* **2009**, *24*, 243.
- [83] P. Krawiec, E. Kockrick, L. Borchardt, D. Geiger, A. Corma, S. Kaskel, *J. Phys. Chem. C* **2009**, *113*, 7755.
- [84] T. Thomberg, A. Jänes, E. Lust, *Electrochim. Acta* **2010**, *55*, 3138.
- [85] S. K. Gordeev, S. A. Kukushkina, A. V. Osipov, Y. V. Pavlov, *Phys. Solid State* **2000**, *42*, 2314.
- [86] Y. Gogotsi, A. Nikitin, H. Ye, W. Zhou, J. E. Fischer, B. Yi, H. C. Foley, M. W. Barsoum, *Nat. Mater.* **2003**, *2*, 591.
- [87] S. Urbonaitė, J. M. Juárez-Galán, J. Leis, F. Rodríguez-Reinoso, G. Svensson, *Microporous Mesoporous Mater.* **2008**, *113*, 14.
- [88] J. C. Palmer, A. Llobet, S.-H. Yeon, J. E. Fischer, Y. Shi, Y. Gogotsi, K. E. Gubbins, *Carbon* **2010**, *48*, 1116.
- [89] J. C. Palmer, S. J. Jain, K. E. Gubbins, J. E. Fischer, R. K. Dash, Y. Gogotsi, in *Characterization of Porous Solids VIII*, (Eds: S. Kaskel, P. Llewellyn, F. Rodriguez-Reinoso, N. A. Seaton), RSC Publishing, Cambridge **2009**, p56.
- [90] Y. G. Gogotsi, S. Welz, D. A. Ersoy, M. J. McNallan, *Nature* **2001**, *411*, 283.
- [91] E. Smorgonskaya, R. Kyutt, A. Danishevskii, C. Jardin, R. Meaudre, O. Marty, S. Gordeev, A. Grechinskaya, *J. Non-Cryst. Solids* **2002**, *299–302*, 810.
- [92] S. Welz, Y. Gogotsi, M. J. McNallan, *J. Appl. Phys.* **2003**, *93*, 4207.
- [93] O. E. Babkin, G. K. Ivakhnyuk, Y. N. Lukin, N. F. Fedorov, *Zh. Prikl. Khim* **1984**, *57*, 1719.
- [94] J. Zheng, T. C. Ekström, S. K. Gordeev, M. Jakob, *J. Mater. Chem.* **2000**, *10*, 1039.
- [95] H. P. Boehm, *Carbon* **1997**, *35*, 581.
- [96] M. Jacob, U. Palmqvist, P. C. A. Alberius, T. C. Ekström, M. Nygren, S. Lidin, *Solid State Sci.* **2003**, *5*, 133.
- [97] A. Perkson, J. Leis, M. Arelupp, M. Käärik, S. Urbonaitė, G. Svensson, *Carbon* **2003**, *41*, 1729.
- [98] S. Dimovski, A. Nikitin, H. Ye, Y. Gogotsi, *J. Mater. Chem.* **2004**, *14*, 238.
- [99] K. W. Adu, S. C. Desai, A. N. Sidorov, G. U. Sumanasekera, A. D. Lueking, *Langmuir* **2009**, *25*, 582.
- [100] G. Yushin, R. Dash, J. Jagiello, J. E. Fischer, Y. Gogotsi, *Adv. Funct. Mater.* **2006**, *16*, 2288.
- [101] J. Leis, M. Arulepp, A. Kuura, M. Lätt, E. Lust, *Carbon* **2006**, *44*, 2122.
- [102] Y. A. Maletin, N. G. Strizhakova, V. G. Izotov, A. A. Mironova, S. G. Kozachkov, V. G. Danilin, S. N. Podmogilny, M. Arulepp, J. A. Kukushkina, A. E. Kravtjik, V. V. Sokolov, A. Perkson, J. Leis, J. Zheng, S. K. Gordeev, J. Y. Kolotilova, J. Cederstrom, C. L. Wallace, *Patent WO 02/39468*, **2002**.
- [103] Y. A. Maletin, N. Strizhakova, S. Kozachkov, A. Mironova, S. Podmogilny, V. Danilin, J. Kolotilova, V. Izotov, G. S. Konstantinovich, J. K. Aleksandrovna, V. S. Vasileviti, A. K. Efi Movitj, A. Perkson, M. Arulepp, J. Leis, C. L. Wallace, J. Zheng, *US Patent 6697249*, **2004**.
- [104] J. Leis, M. Arulepp, A. Perkson, *Patent WO/2004/094307*, **2004**.
- [105] Y. G. Gogotsi, M. Yoshimura, *Nature* **1994**, *367*, 628.
- [106] Y. G. Gogotsi, M. Yoshimura, *MRS Bull.* **1994**, *10*, 39.
- [107] Y. G. Gogotsi, P. Kofstad, M. Yoshimura, K. G. Nickel, *Diamond Relat. Mater.* **1996**, *5*, 151.
- [108] Y. G. Gogotsi, K. G. Nickel, D. Bahloul-Hourlier, T. Merle-Mejean, G. E. Khomenko, K. Skjerlie, *J. Mater. Chem.* **1996**, *6*, 595.
- [109] S. Kitaoka, T. Tsuji, T. Katoh, Y. Yamaguchi, K. Kashiwagi, *J. Am. Ceram. Soc.* **1994**, *77*, 1851.
- [110] N. S. Jacobson, Y. G. Gogotsi, M. Yoshimura, *J. Mater. Chem.* **1995**, *5*, 595.
- [111] S. Ito, M. Tomozawa, *J. Am. Ceramic Soc.* **1981**, *64*, C160.
- [112] G. Perera, R. H. Doremus, W. Lanford, *J. Am. Ceramic Soc.* **1991**, *74*, 1269.
- [113] N. S. Jacobson, Y. G. Gogotsi, M. Yoshimura, *J. Mater. Chem.* **1995**, *5*, 595.
- [114] K. G. Nickel, Y. G. Gogotsi, in *Handbook of Ceramic Hard Materials*, Vol. 1 (Ed: R. Riedel), Wiley-VCH Verlag, Weinheim, Germany **2000**, 374.
- [115] Y. G. Gogotsi, M. Yoshimura, *Nature* **1994**, *367*, 628.
- [116] Y. G. Gogotsi, M. Yoshimura, *J. Mater. Sci. Lett.* **1995**, *14*, 755.
- [117] T. Kraft, K. G. Nickel, Y. G. Gogotsi, *J. Mater. Sci.* **1998**, *33*, 4357.
- [118] Y. G. Gogotsi, in *Advanced Multilayered and Fibre-Reinforced Composites*, (Ed: Y. M. Haddad), Kluwer Academic Publishers, Dordrecht, Germany **1998**, 217.

- [119] T. Kraft, K. G. Nickel, *J. Mater. Chem.* **2000**, *10*, 671.
- [120] R. Roy, D. Ravichandran, A. Badzian, E. Breval, *Diamond Relat. Mater.* **1996**, *5*, 973.
- [121] K. G. Nickel, T. Kraft, Y. G. Gogotsi, in *Handbook of Ceramic Hard Materials*, (Ed: R. Riedel), Wiley, Weinheim, Germany **2000**, 374.
- [122] H. Zhang, V. Presser, C. Berthold, K. G. Nickel, X. Wang, C. Raisch, T. Chasse, L. He, Y. Zhou, *J. Am. Ceramic Soc.* **2010**, *93*, 1148.
- [123] B. Basavalingu, J. M. Calderon-Moreno, K. Byrappa, Y. G. Gogotsi, M. Yoshimura, *Carbon* **2001**, *39*, 1763.
- [124] B. Basavalingu, P. Madhusudan, A. S. Dayananda, K. Lal, K. Byrappa, M. Yoshimura, *J. Mater. Sci.* **2008**, *43*, 2153.
- [125] Y. Gogotsi, J. A. Libera, M. Yoshimura, in *Perspectives in Fullerene Nanotechnology*, (Ed: E. Osawa), Kluwer, Dordrecht, Germany **2001**, 253.
- [126] T. Y. Kosolapova, *Carbides. Properties, Production, and Applications*, Plenum Press, New York **1971**.
- [127] L. M. Foster, G. Long, H. C. Stumpf, *The American Mineralogist* **1958**, *43*, 285.
- [128] N. I. Voronin, V. L. Kuznetsova, R. I. Bresker, *Ogneupory* **1965**, *30*, 22.
- [129] N. I. Voronin, V. L. Kuznetsova, R. I. Bresker, in *Silicon Carbide*, (Ed: I. N. Frantsevich), Consultants Bureau, New York **1970**, 81.
- [130] G. Busch, *Helv. Phys. Acta* **1946**, *19*, 167.
- [131] A. Braun, G. Busch, *Helv. Phys. Acta* **1947**, *20*, 33
- [132] F. Euler, E. R. Czerlinsky, in *Silicon Carbide. A High Temperature Semiconductor. Proceedings of the Conference*, (Eds: J. R. O'Connor, J. Smiltens), Pergamon Press, Oxford **1960**, 155.
- [133] D. V. Badami, *Carbon* **1965**, *3*, 53.
- [134] S. Iijima, *J. Solid State Chem.* **1982**, *42*, 101.
- [135] J. Comer, *J. Appl. Crystallography* **1971**, *4*, 12.
- [136] D. V. Badami, *Nature* **1962**, *193*, 569.
- [137] F. Meyer, G. J. Loyen, *Acta Electronica* **1975**, *18*, 33.
- [138] W. J. Choyke, H. Matsunami, G. Pensl, *Silicon Carbide. Recent Major Advances*, Springer, Berlin **2004**.
- [139] R. A. Stein, P. Lanig, S. Leibenzeder, *Mater. Sci. and Eng. B* **1992**, *B11*, 69.
- [140] S. Irle, Z. Wang, G. S. Zheng, K. Morokuma, M. Kusunoki, *J. Chem. Phys.* **2006**, *125*, 044702.
- [141] A. V. Zinovev, J. F. Moore, J. Hryn, M. J. Pellin, *Surf. Sci.* **2006**, *600*, 2242.
- [142] M. Kusunoki, T. Suzuki, T. Hirayama, N. Shibata, *Physica B* **2002**, *323*, 296.
- [143] M. Kusunoki, J. Shibata, M. Rokkaku, T. Hirayama, *Jpn. J. Appl. Phys.* **1998**, *37*, L605.
- [144] M. Kusunoki, T. Suzuki, K. Kaneko, M. Ito, *Philos. Mag. Lett.* **1999**, *79*, 153.
- [145] M. Kusunoki, T. Suzuki, T. Hirayama, N. Shibata, K. Kaneko, *Appl. Phys. Lett.* **2000**, *77*, 531.
- [146] M. Kusunoki, T. Saito, Y. Ikuhara, *Jpn. Fine Ceram. Center Rev.* **1997**, *9*, 248.
- [147] T. Shimizu, Y. Ishikawa, M. Kusunoki, T. Nagano, N. Shibata, *Jpn. J. Appl. Phys.* **2000**, *39*, L1057.
- [148] H. Takikawa, R. Miyano, M. Yatsuki, T. Sakakibara, *Jpn. J. Appl. Phys. Part 2-Lett.* **1998**, *37*, L187.
- [149] S. Botti, R. Ciardi, L. Asilyan, L. De Dominicis, F. Fabbri, S. Orlanducci, A. Fiori, *Chem. Phys. Lett.* **2004**, *400*, 264.
- [150] A. Watanabe, Y. Hisada, S. Mukainakano, N. Tanaka, *J. Microsc.* **2001**, *203*, 40.
- [151] T. Nagano, Y. Ishikawa, S. Noriyoshi, *Jpn. J. Appl. Phys.* **2003**, *42*, 1380.
- [152] Z. Wang, S. Irle, G. Zheng, M. Kusunoki, K. Morokuma, *J. Phys. Chem. C* **2007**, *111*, 12960.
- [153] N. G. Wright, C. M. Johnson, A. G. O'Neill, *Mater. Sci. Eng. B* **1999**, *B61–62*, 468.
- [154] K. Christiansen, R. Helbig, *J. Appl. Phys.* **1996**, *79*, 3276.
- [155] H. Konishi, H. Matsuoka, N. Toyama, M. Naitoh, S. Nishigaki, M. Kusunoki, *Thin Solid Films* **2004**, *464*, 295
- [156] P. N. First, W. A. De Heer, T. Seyller, C. Berger, J. A. Stroschio, J.-S. Moon, *MRS Bulletin* **2010**, *35*, 296.
- [157] J. Robinson, X. Weng, K. Trumbull, R. Cavaleiro, M. Wetherington, E. Frantz, M. Labella, Z. Hughes, M. Fanton, D. Snyder, *ACS Nano* **2010**, *4*, 153.
- [158] S. Pathak, Z. G. Cambaz, S. R. Kalidindi, J. G. Swadener, Y. Gogotsi, *Carbon* **2009**, *47*, 1969.
- [159] G. Toth, J. Mäklin, N. Halonen, J. Palosaari, J. Juuti, H. Janutunen, K. Kordas, W. G. Sawyer, R. Vajtai, P. Ajayan, *Adv. Mater.* **2009**, *21*, 2054.
- [160] A. J. Van Bommel, J. E. Crombeen, A. Van Tooren, *Surf. Sci.* **1975**, *48*, 463.
- [161] E. Rollings, G.-H. Gweon, S. Y. Zhou, B. S. Mun, J. L. Mc-Chesney, B. S. Hussain, A. V. Fedorov, P. N. First, W. A. de Heer, A. Lanzara, *J. Phys. Chem. Solids* **2006**, *67*, 2172.
- [162] C. Virojanadara, M. Syväjarvi, R. Yakimova, L. I. Johansson, A. A. Zakharov, T. Balasubramanian, *Phys. Rev. B* **2008**, *78*, 245403.
- [163] S. Mouras, A. Hamma, D. Djurado, J.-C. Cousseins, *Rev. Chim. Miner.* **1987**, *24*, 572.
- [164] C. Berger, Z. Song, T. Li, X. Li, A. Y. Obgbazghi, R. Feng, Z. Dai, A. N. Marchenkov, E. H. Conrad, P. N. First, W. A. De Heer, *J. Phys. Chem. B* **2004**, *108*, 19912.
- [165] P. Sutter, *Nat. Mater.* **2009**, *8*, 171.
- [166] M. Hupalo, E. H. Conrad, E. M. Tringides, *Phys. Rev. B* **2001**, *80*, 041401R.
- [167] L. I. Johansson, P. A. Glans, A. N. A. Hellgren, *Surf. Sci.* **1998**, *405*, 288.
- [168] V. Derycke, R. Martel, M. Radosavljevic, F. M. Ross, P. Avouris, *Nano Lett.* **2002**, *2*, 1043.
- [169] M. I. Bolen, S. E. Harrison, L. B. Biedermann, M. A. Capano, *Phys. Rev. B* **2009**, *80*, 115433.
- [170] J. B. Hannon, R. M. Tromp, *Phys. Rev. B* **2008**, *77*, 241404.
- [171] F. Varchon, R. Feng, J. Hass, X. Li, B. N. Nguyen, C. Naud, P. Mallet, J.-Y. Veuillen, C. Berger, E. H. Conrad, L. Magaud, *Phys. Rev. Lett.* **2007**, *99*.
- [172] A. Charrier, A. Coati, T. Argunova, F. Thibaudau, Y. Garreau, R. Pinchaux, I. Forbeaux, J. M. Debever, M. Sauvage-Simkin, J. M. Themlin, *J. Appl. Phys.* **2002**, *92*, 2479.
- [173] K. V. Emtsev, F. Speck, T. Seyller, L. Ley, J. D. Riley, *Phys. Rev. B* **2008**, *77*, 155303.
- [174] G. M. Rutter, N. P. Guisinger, J. N. Crain, E. A. A. Jarvis, M. D. Stiles, T. Li, P. N. First, J. A. Stroschio, *Phys. Rev. B* **2007**, *76*, 235416.
- [175] D. L. Nika, S. Ghosh, E. P. Pokatilov, A. A. Balandin, *Appl. Phys. Lett.* **2010**, *94*, 203131.
- [176] B. Partoens, F. M. Peeters, *Phys. Rev. B* **2006**, *74*, 075404.
- [177] B. L. VanMil, R. L. Myer-Ward, J. L. Tedesco, C. R. Eddy, G. G. Jernigan, J. C. Culbertson, P. M. Campbell, J. M. McCrate, S. A. Kitt, D. K. Gaskill, *Mater. Sci. Forum* **2009**, *615–617*, 211.
- [178] R. M. Tromp, J. B. Hannon, *Phys. Rev. Lett.* **2009**, *102*, 106104.
- [179] H. Huang, W. Chen, S. Chen, A. T. S. Wee, *ACS Nano* **2009**, *2*, 2513.
- [180] T. C. Chandler, M. B. Lari, T. S. Sudarshan, *Mater. Sci. Forum* **2000**, *338–342*, 845.
- [181] J. R. Grim, M. Benamara, M. Skowronski, W. J. Everson, V. D. Heydemann, *Semicond. Sci. Technol.* **2006**, *21*, 1709.
- [182] M. Kikuchi, Y. Takahashi, T. Suga, S. Suzuki, Y. Bando, *J. Am. Ceram. Soc.* **1992**, *75*, 189.
- [183] Y. C. Lin, C. H. Kao, *Int. J. Adv. Manuf. Technol.* **2005**, *25*, 33.
- [184] F. Owman, C. Hallin, P. Martensson, E. Janzen, *J. Cryst. Growth* **1996**, *167*, 391.
- [185] P. Vicente, D. Chaussende, *II-Vs Review* **2002**, *15*, 46.
- [186] G. A. H. de Mesquita, *Acta Crystallog.* **1967**, *610*.

- [187] C. Virojanadara, R. Yakimova, J. R. Osiecki, M. Syväjärvi, R. I. G. Uhrberg, A. A. Zakharov, *Surf. Sci.* **2009**, *603*, L87.
- [188] Z. Ni, Y. Wang, T. Yu, Z. Shen, *Nano Res.* **2008**, *1*, 273.
- [189] R. Yang, Q. S. Huang, X. L. Chen, G. Y. Zhang, H.-J. Gao, *J. Appl. Phys.* **2010**, *107*, 034305/1.
- [190] E. Johansson, B. Hjorvarsson, T. Ekström, M. Jacob, *J. Alloys Compd.* **2002**, *330–332*, 670.
- [191] A. Jerome, US Patent 2005/0058875, **2005**.
- [192] P. Simon, A. Burke, *Electrochem. Soc. Interface* **2010**, *17*, 38.
- [193] F. I. Simjee, P. H. Chou, *IEEE Trans. Power Electron.* **2008**, *23*, 1526.
- [194] A. Burke, *J. Power Sources* **2000**, *91*, 37.
- [195] R. Dash, J. Chmiola, G. Yushin, Y. Gogotsi, G. Laudisio, J. Singer, J. Fischer, S. Kucheyev, *Carbon* **2006**, *44*, 2489.
- [196] R. Lin, P. L. Taberna, J. Chmiola, D. Guay, Y. Gogotsi, P. Simon, *J. Electrochem. Soc.* **2009**, *156*, A7.
- [197] J. Segalini, B. Daffos, P. L. Taberna, Y. Gogotsi, P. Simon, *Electrochem. Acta* **2010**, *55*, 7489.
- [198] C. Portet, M. Á. Lillo-Ródenas, A. Linares-Solano, Y. Gogotsi, *Phys. Chem. Chem. Phys.* **2009**, *11*, 4943.
- [199] C. Portet, G. Yushin, Y. Gogotsi, *J. Electrochem. Soc.* **2008**, *155*, A531.
- [200] T. Thomberg, A. Jänes, E. Lust, *J. Electroanal. Chem.* **2009**, *630*, 55.
- [201] J. A. Fernandez, M. Arulepp, J. Leis, F. Stoeckli, T. A. Centeno, *Electrochim. Acta* **2008**, *53*, 7111.
- [202] J. Chmiola, G. Yushin, Y. Gogotsi, C. Portet, P. Simon, P. L. Taberna, *Science* **2006**, *313*, 1760.
- [203] H. Shi, *Electrochim. Acta* **1996**, *41*, 1633.
- [204] J. Chmiola, C. Largeot, P. L. Taberna, P. Simon, Y. Gogotsi, *Angew. Chem Int. Ed.* **2008**, *47*, 3392.
- [205] C. Largeot, C. Portet, J. Chmiola, P.-L. Taberna, Y. Gogotsi, P. Simon, *J. Am. Chem. Soc.* **2008**, *130*, 2730.
- [206] M. Arulepp, J. Leis, M. Latt, F. Miller, K. Rumma, E. Lust, A. F. Burke, *J. Power Sources* **2006**, *162*, 1460.
- [207] E. Lust, A. Jänes, M. Arulepp, *J. Electroanal. Chem.* **2004**, *562*, 33.
- [208] S. K. Gordeev, A. V. Vartanova, *Zh. Prikl. Khim* **1994**, *67*, 1375.
- [209] S. K. Gordeev, A. V. Vartanova, *Zh. Prikl. Khim* **1994**, *67*, 1080.
- [210] R. G. Avarbz, A. V. Vartanova, S. K. Gordeev, S. G. Zjukov, B. A. Zelenov, A. E. Kravtjik, V. P. Kuznetsov, J. A. Kususjkina, T. V. Mazaeva, O. S. Pankina, V. V. Sokolov, US Patent 6110335, **2000**.
- [211] S. K. Gordeev, A. V. Vartanova, *Zh. Prikl. Khim* **1991**, *64*, 1178.
- [212] I. M. Kotina, V. M. Lebedev, A. G. Ilves, G. V. Patsekina, L. M. Tuhkonen, S. K. Gordeev, M. A. Yagovkina, T. Ekström, *J. Non-Cryst. Solids* **2002**, *299–302*, 820.
- [213] I. M. Kotina, V. M. Lebedev, A. G. Ilves, G. V. Patsekina, L. M. Tuhkonen, S. K. Gordeev, M. A. Yagovkina, T. Ekström, *J. Non-Cryst. Solids* **2002**, *299–302*, 815.
- [214] H. S. Moon, J. M. Kim, Y. J. Kim, Korean Patent 2007–5625 20070118, **2008**.
- [215] B. A. Anderson, E. J. Nowak, US Patent US007732859, **2007**.
- [216] T. Ihn, J. Güttinger, F. Molitor, S. Schnez, E. Schurtenberger, A. Jacobsen, S. Hellmüller, T. Frey, S. Dröschner, C. Stampfer, K. Ensslin, *Mater. Today* **2010**, *13*, 44.
- [217] J. Kedzierski, P.-L. Hsu, P. Healey, P. W. Wyatt, C. L. Keast, M. Sprinkle, C. Berger, W. A. de Heer, *IEEE Trans. Electron Devices* **2008**, *55*, 2078.
- [218] J. S. Moon, D. Curtis, M. Hu, D. Wong, C. McGuire, P. M. Campbell, G. Jernigan, J. L. Tedesco, B. VanMil, R. Myers-Ward, C. Eddy, D. K. Gaskill, *IEEE Electron Device Lett.* **2009**, *30*, 650.
- [219] K. S. Novoselov, A. K. Geim, S. V. Morozov, D. Jiang, Y. Zhang, S. V. Dobonos, I. V. Grigorieva, A. A. Firsov, *Science* **2004**, *306*, 666.
- [220] M. Lemme, T. J. Echtermeyer, M. Baus, H. Kurz, *IEEE Electron Device Lett.* **2007**, *28*, 282.
- [221] X. Li, X. Wu, M. Sprinkle, F. Ming, M. Ruan, Y. Hu, C. Berger, W. A. de Heer, *Phys. Status Solidi (A)* **2010**, *207*, 286.
- [222] S. Odaka, H. Miyazaki, S.-L. Li, A. Kanda, K. Morita, S. Tanaka, Y. Miyata, H. Kataura, K. Tsukagoshi, Y. Aoyagi, *Appl. Phys. Lett.* **2010**, *96*, 062111/1.
- [223] K. I. Bolotin, K. J. Sikes, J. Hone, H. L. Stormer, P. Kim, *Phys. Rev. Lett.* **2008**, *101*, 096802.
- [224] M. D. Stoller, S. Park, Y. Zhu, J. An, R. S. Ruoff, *Nano Lett.* **2008**, *8*, 3498.
- [225] D. Pech, M. Brunet, H. Durou, P. Huan, V. Mochalin, Y. Gogotsi, P.-L. Taberna, P. Simon, *Nat. Nanotechnol.* **2010**, *5*, 641.
- [226] J. R. Miller, R. A. Outlaw, B. C. Holloway, *Science* **2010**, *329*, 1637.
- [227] Y. Gogotsi, R. K. Dash, G. Yushin, T. Yildirim, G. Laudisio, J. E. Fischer, *J. Am. Chem. Soc.* **2005**, *127*, 16006.
- [228] S.-H. Yeon, S. Osswald, Y. Gogotsi, J. P. Singer, J. M. Simmons, J. E. Fischer, M. Á. Lillo-Ródenas, A. Linares-Solano, *J. Power Sources* **2009**, *191*, 560.
- [229] S. Ma, D. Sun, J. M. Simmons, C. D. Collier, D. Yuan, H.-C. Zhou, *J. Am. Chem. Soc.* **2008**, *130*, 1012.
- [230] B. Carroll, Y. Gogotsi, A. Kovalchenko, A. Erdemir, M. J. McNallan, *Tribology Lett.* **2003**, *15*, 51.
- [231] D. A. Ersoy, M. J. McNallan, Y. Gogotsi, A. Erdemir, *Tribol. Trans.* **2000**, *43*, 809.
- [232] L. Chen, H. Ye, Y. Gogotsi, *J. Am. Ceram. Soc.* **2003**, *86*, 1830.
- [233] L. Chen, H. Ye, Y. Gogotsi, *Int. J. Appl. Ceram. Technol.* **2004**, *1*, 68.
- [234] D. A. Ersoy, M. J. McNallan, Y. Gogotsi, *J. Electrochem. Soc.* **2001**, *148*, C774.
- [235] Y. A. Elabd, Y. Gogotsi, B. Eirich, D. Shay US Patent US 2010/0285392, **2010**.
- [236] S. Yachamaneni, G. Yushin, S.-H. Yeon, Y. Gogotsi, C. Howell, S. Sandeman, G. Phillips, S. V. Mikhalovsky, *Biomaterials* **2010**, *31*, 4789.
- [237] A. Jänes, H. Kurig, E. Lust, *Carbon* **2007**, *45*, 1226.